iScience

CellPress
OPEN ACCESS

Article

Divergent input patterns to the central lateral amygdala play a duet in fear memory formation

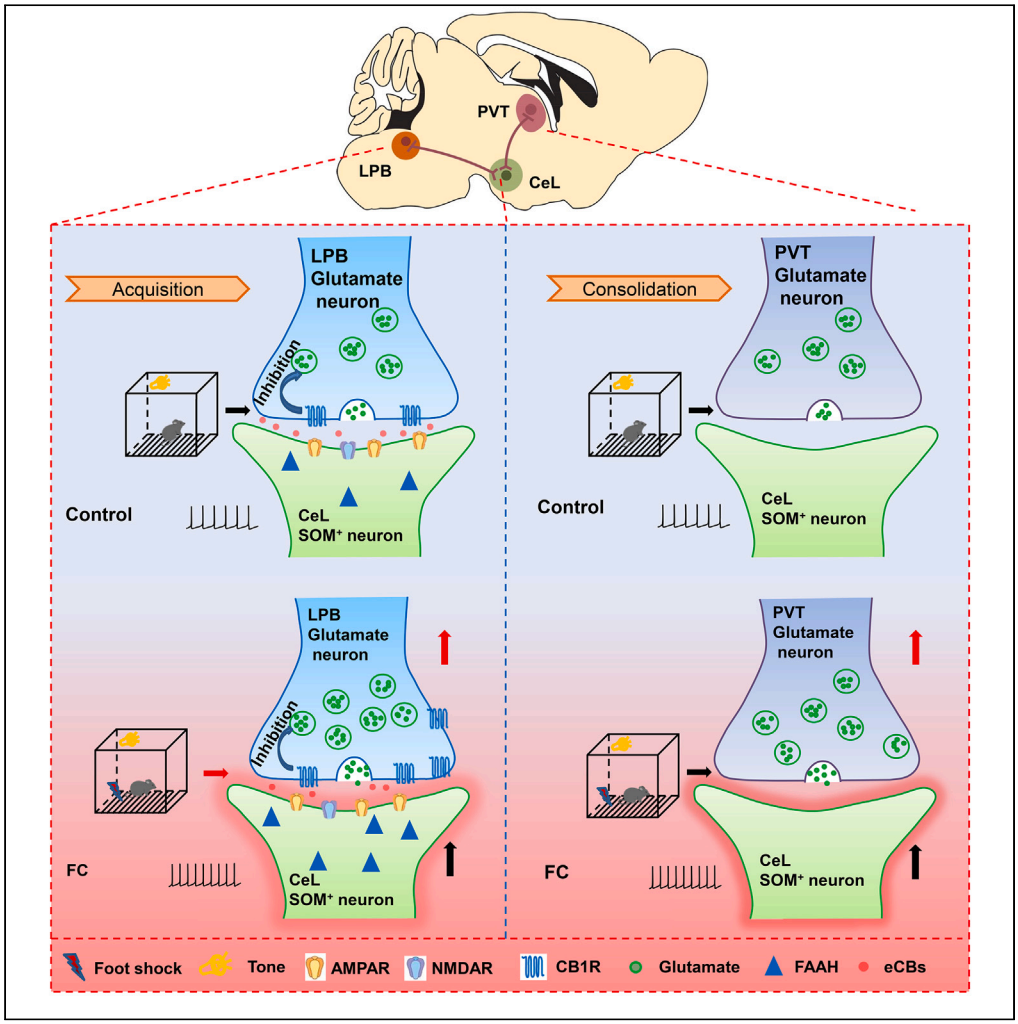

Jing-hua Gao, Yue-ying Liu, Hui-xiang Xu, ..., Jun-li Cao, Rong Hua, Yong-mei Zhang

caojl0310@aliyun.com (J.-l.C.)
ilovezq@yeah.net (R.H.)
zhangym700@163.com (Y.-m.Z.)

Highlights

SOM-positive GABAergic neurons in the CeL were involved in fear memory acquisition

Activation of the LPB^{Glu}→CeL^{SOM} pathway promotes fear memory acquisition

The PVT^{Glu}→CeL^{SOM} pathway are expected to interfere with consolidation-related processes

CB1Rs at the LPB^{Glu}→CeL^{SOM} terminals participate in cannabinoid-induced impairments in fear memory acquisition

Gao et al., iScience 27, 110886
October 18, 2024
https://doi.org/10.1016/j.isci.2024.110886

iScience

CellPress
OPEN ACCESS

Article

Divergent input patterns to the central lateral amygdala play a duet in fear memory formation

Jing-hua Gao,[1,5,7] Yue-ying Liu,[1,2,3,6,7] Hui-xiang Xu,[1,2,3,7] Ke Wu,[1,2,3] Le-le Zhang,[1,2,3] Peng Cheng,[1,2,3,6] Xiao-han Peng,[1,2,3] Jun-li Cao,[1,2,3,6,*] Rong Hua,[4,*] and Yong-mei Zhang[1,2,3,6,8,*]

SUMMARY

Somatostatin (SOM)-expressing neurons in the central lateral amygdala (CeL) are responsible for fear memory learning, but the circuit and molecular mechanisms underlying this biology remain elusive. Here, we found that glutamatergic neurons in the lateral parabrachial nucleus (LPB) directly dominated the activity of CeL^{SOM} neurons, and that selectively inhibiting the LPB^{Glu} → CeL^{SOM} pathway suppressed fear memory acquisition. By contrast, inhibiting CeL-projecting glutamatergic neurons in the paraventricular thalamic nucleus (PVT) interfered with consolidation-related processes. Notably, CeL^{SOM}-innervating neurons in the LPB were modulated by presynaptic cannabinoid receptor 1 (CB1R), and knock down of CB1Rs in LPB glutamatergic neurons enhanced excitatory transmission to the CeL and partially rescued the impairment in fear memory induced by CB1R activation in the CeL. Overall, our study reveals the mechanisms by which CeL^{SOM} neurons mediate the formation of fear memories during fear conditioning in mice, which may provide a new direction for the clinical research of fear-related disorders.

INTRODUCTION

Fear refers to an adaptive response that can be rapidly generated by individuals when confronted with threatening contexts and cues. Fear can be divided into innate fear and learned fear. Innate fear includes responses elicited by predators, heights, pain, fast approaching objects, and primal threats like snakes and spiders. Learned fear is developed through acquired experiences, characterized by the fear responses to the specific context and related cues following exposure to a traumatic event, thereby leads to the formation of conditioned fear memories.[1,2] fear conditioning (FC) has been widely employed in animal studies to investigate the mechanisms underlying the formation of fear memories.[3,4] Psychological interventions directed at the trauma-related memories can be effective in treating fear-related disorders, significantly mitigating patients' symptoms and improving their prognosis, whereas effective pharmacotherapies targeting the neurobiological mechanisms have not yet been discovered.[5]

The neurobiological mechanisms underlying different stages of fear memory formation have been extensively characterized in rodents exposed to FC. The formation of fear memories includes the processes of acquisition, consolidation, and reconsolidation.[6] The primary brain regions involved in fear memory formation include the amygdala, the hippocampus, and the medial prefrontal cortex; among these, the amygdala is the integration center for sensory information during the formation of auditory fear memories.[6,7] The central lateral amygdala (CeL) is the output subnucleus of the amygdala and is critical for fear memory formation.[8–11] Previous work has demonstrated a significant increase in the frequency of miniature excitatory postsynaptic currents (mEPSCs) recorded from somatostatin (SOM)-positive neurons in the CeL after FC, indicating enhanced excitatory synaptic transmission onto CeL-SOM^{+} neurons.[9,12] Anatomical studies have shown that the CeL receives direct glutamatergic projections from several emotion-associated brain sites, including the lateral parabrachial nucleus (LPB) and the paraventricular thalamic nucleus (PVT).[8] Notably, the LPB and PVT play important roles in the transmission of nociceptive information and have been shown to be involved in the processing of stress responses and the gating of fear memory expression.[13,14] Therefore, the molecular mechanisms underlying the excitatory LPB → CeL and PVT → CeL projections that modulate fear memory formation are of great interest.

Cannabinoid type 1 receptors, as the most abundant seven transmembrane G-protein-coupled presynaptic receptors in the mammalian brain, are receiving increasing attention due to their important roles in modulating synaptic plasticity.[15,16] CB1R functions as a neuromodulator through retrograde signaling, with those located at glutamatergic and GABA (γ-aminobutyric acid) synapses mediating depression of

[1]NMPA Key Laboratory for Research and Evaluation of Narcotic and Psychotropic Drugs, Xuzhou 221002, Jiangsu, China
[2]Jiangsu Province Key Laboratory of Anesthesia and Analgesia Application Technology, Xuzhou Medical University, Xuzhou 221002, Jiangsu, China
[3]Jiangsu Province Key Laboratory of Anesthesiology, Xuzhou Medical University, Xuzhou 221002, Jiangsu, China
[4]Department of Emergency, The Affiliated Hospital of Xuzhou Medical University, Xuzhou 221004, Jiangsu, China
[5]Department of Anesthesiology, The Yancheng Clinical College of Xuzhou Medical University, The First People's Hospital of Yancheng, Yancheng 224008, Jiangsu, China
[6]Present address: 209 Tongshan Road, Xuzhou, Jiangsu 221002, China
[7]These authors contributed equally
[8]Lead contact
*Correspondence: caojl0310@aliyun.com (J.-l.C.), ilovezq@yeah.net (R.H.), zhangym700@163.com (Y.-m.Z.)
https://doi.org/10.1016/j.isci.2024.110886

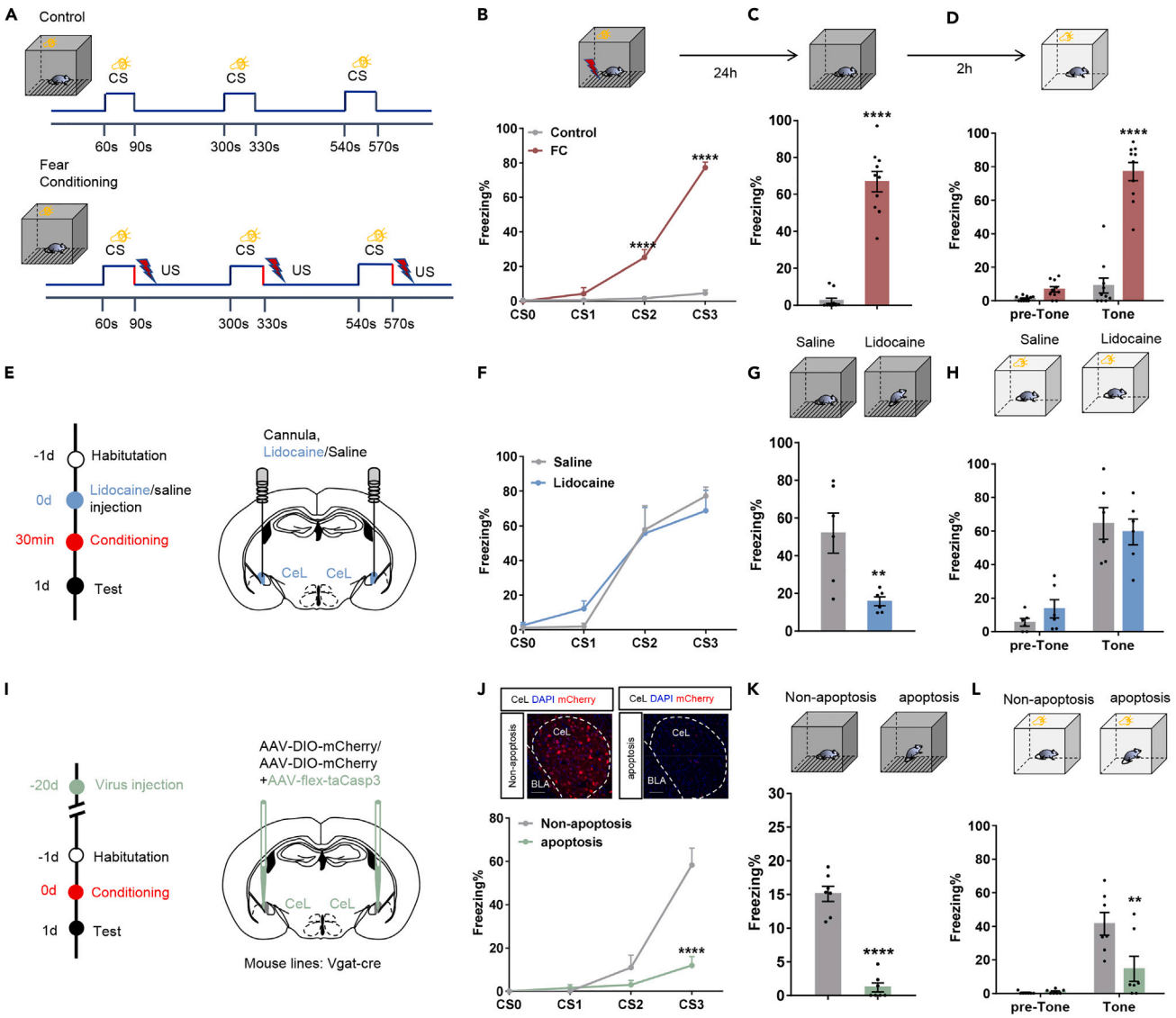

Figure 1. CeL GABAergic neurons are involved in fear conditioning

(A) Experimental paradigm for fear conditioning.

(B) Mice presented with three CS–US pairings exhibited increased freezing levels compared with mice merely exposed to the CSs (two-way ANOVA, group: $F_{(1,18)} = 144.4$, ****$p < 0.0001$; time: $F_{(3,54)} = 131.2$, ****$p < 0.0001$; interaction: $F_{(3,54)} = 105.8$, ****$p < 0.0001$; Bonferroni's post hoc test, for Control versus FC at CS2, ****$p < 0.0001$; For Control versus FC at CS3, ****$p < 0.0001$; $n = 10$ mice).

(C and D) FC mice exhibited increased freezing levels during contextual (C, two-sided unpaired *t*-test, $t_{(1/18)} = 11.23$, ****$p < 0.0001$, $n = 10$ mice) and cued (D, two-way ANOVA, group: $F_{(1,18)} = 85.66$, ****$p < 0.0001$; time: $F_{(1,18)} = 147.7$, ****$p < 0.0001$; interaction: $F_{(1,18)} = 94.8$, ****$p < 0.0001$; Bonferroni's post hoc test, for Control versus FC during tone presentation, ****$p < 0.0001$; $n = 10$ mice) fear memory recall compared with the Control mice.

(E) Time course (left) and coronal schematic (right) of CeL-infusion of saline or lidocaine.

(F–H) Disruption of neuronal excitability within the CeL via lidocaine did not exert effects on freezing responses during fear conditioning (F, two-way ANOVA, group: $F_{(1,10)} = 0.001$, $p = 0.973$; time: $F_{(3,30)} = 49.29$, ****$p < 0.0001$; interaction: $F_{(3,30)} = 0.5976$, $p = 0.6215$; $n = 6$ mice) or in the cued fear memory test (H, two-way ANOVA, group: $F_{(1,10)} = 0.040$, $p = 0.8463$; time: $F_{(1,10)} = 92.66$, ****$p < 0.0001$; interaction: $F_{(1,10)} = 1.432$, $p = 0.259$. $n = 6$ mice), but it did suppress freezing behaviors during the context exposure sessions (G, two-sided unpaired *t*-test, $t_{(1/10)} = 3.349$, **$p = 0.0074$, $n = 6$ mice).

(I) Time course (left) and schematic diagram (right) of bilateral CeL injection of taCasp3 virus.

(J) Top, Representative confocal images show a marked decrease in the number of GABAergic neurons in the CeL after taCasp3 injection. Scale bar, 50 μm. Bottom, Ablation of GABAergic neurons in the CeL produced a reliable decrease in freezing levels during the last session of fear conditioning (two-way ANOVA, group: $F_{(1,12)} = 41.64$, ****$p < 0.0001$; time: $F_{(3,36)} = 32.63$, ****$p < 0.0001$; interaction: $F_{(3,36)} = 15.11$, ****$p < 0.0001$; Bonferroni's post hoc test, freezing for Non-apoptosis versus apoptosis at CS3, ****$p < 0.0001$; $n = 7$ mice).

Figure 1. *Continued*

(K and L) Mice that received intra-CeL injections of taCasp3 virus showed impaired fear memory recall in the contextual fear test (K, two-sided unpaired *t*-test, $t_{(1/12)} = 10.54$, ****$p < 0.0001$, $n = 7$ mice) and in the cued fear memory test (L, two-way ANOVA, group: $F_{(1,12)} = 7.141$, *$p = 0.02$; time: $F_{(1,12)} = 28.44$, ***$p = 0.0002$; interaction: $F_{(1,12)} = 7.202$, *$p = 0.02$; Bonferroni's post hoc test, freezing for Non-apoptosis versus apoptosis during Tone presentation, **$p = 0.0018$; $n = 7$ mice). All of the data are presented as mean ± SEM. *$p < 0.05$, **$p < 0.01$, ****$p < 0.0001$.

presynaptic transmitter release via combination with endocannabinoids synthesized by postsynaptic neurons, so as to induce depolarization-induced suppression of excitation (DSE) and depolarization-induced suppression of inhibition (DSI).[17] CB1R deficiency can result in enhanced contextual fear memory acquisition and impaired fear memory extinction in animal models,[18,19] whereas selective activation of CB1Rs in the central nucleus of the amygdala (CeA) inhibits presynaptic glutamate release and disrupts fear memory expression.[20,21] However, the details of the circuit mechanism underlying the regulatory role of CB1Rs in fear memory acquisition remain elusive.

In this study, FC was adopted as an animal model to study the neurobiological mechanisms of fear memory formation.[6,22–24] We employed molecular biology and electrophysiological recordings to explore the role of CeL-GABAergic and SOM^+ GABAergic neurons in fear memory formation, and comprehensively using *in vivo* pharmacological intervention, chemogenetic and optogenetic manipulations to investigate whether the $LPB^{Glu} \rightarrow CeL^{SOM}$ and the $PVT^{Glu} \rightarrow CeL^{SOM}$ pathway were involved in fear memory formation. In addition, electrophysiological recordings combined with optogenetics can dynamically monitor the effects of presynaptic CB1Rs located at excitatory terminals in the CeL on postsynaptic CeL^{SOM} neuronal excitability. Our research revealed the circuit and molecular mechanisms underlying fear memory acquisition, providing an insight for future research on the pathogenesis of fear—related disorders.

RESULTS

Elevated activity of CeL^{GABA} neurons are essential for fear conditioning in mice

A mouse model of FC was established using a protocol modified from previous reports.[22,25] As depicted in Figure 1A, mice were subjected to FC. During the FC, the mice displayed a significant increase in freezing (****$p < 0.0001$, two-way ANOVA test, Figure 1B). On the next day, the mice exhibited enhanced freezing responses when exposed to either the conditioning context (****$p < 0.0001$, two-sided unpaired *t*-test, Figure 1C) or the tone (****$p < 0.0001$, two-way ANOVA test, Figure 1D) during the fear memory testing session.

To gain insights into the nucleus involved in FC, we first examined CeL, a structure that is as important as the basolateral amygdala (BLA) in fear learning and expression.[26,27] Microinjection of lidocaine, a sodium-channel blocker, to transiently inactivate the CeL during FC did not affect the fear responses during the training period or in the cued fear-memory test (Figure 1E; For the training period, $p = 0.973$, two-way ANOVA test; Figure 1F; For the cued test, $p = 0.846$, two-way ANOVA test; Figure 1H); however, it did impair contextual fear memory acquisition, demonstrated by a decrease in freezing levels in the contextual fear-memory test (**$p = 0.0074$, two-sided unpaired *t*-test, Figure 1G). To further validate the role of the CeL in fear memory acquisition, we induced apoptosis in CeL GABAergic neurons, the predominant neuronal population in the CeL,[28,29] by injecting the Cre-dependent taCasp3 virus in Vgat-Cre mice (Figure 1I). Three weeks after virus injection, the number of GABAergic neurons in the CeL was decreased (****$p < 0.0001$, two-sided unpaired *t*-test, Figure S1A). Compared with the control mice, taCasp3-injected mice developed a marked decrease in freezing levels during the FC period, as well as during the context and tone exposure periods in the fear memory tests (For the training period, ****$p < 0.0001$, two-way ANOVA test, Figure 1J; For the contextual test, ****$p < 0.0001$, two-sided unpaired *t*-test; Figure 1K; For the cued test, *$p = 0.02$, two-way ANOVA test; Figure 1L). These preliminary data provide evidence that CeL GABAergic neurons participate in fear memory acquisition, although their exact role remains to be further explored.

Enhanced excitability of CeL^{SOM} neurons in mice exposed to fear conditioning

Given that the GABAergic neurons in the CeL can be divided into multiple neuronal subtypes on the basis of distinct genetic markers,[9–11,30] we wondered whether a specific neuronal subtype mediates CeL-dependent fear memory acquisition. Somatostatin-positive (SOM^+) neurons constitute a major subpopulation within the CeL. These neurons inhibit SOM-negative (SOM^-) neurons and disinhibit output neurons in the medial central amygdala (CeM), thereby facilitating the generation of conditioned responses.[9,31] To characterize the precise role of CeL^{SOM} neurons in fear memory acquisition, we measured changes in their excitability following FC. SOM^+ neurons were identified by injecting AAV-SST (Somatostatin)-mCherry into the CeL (Figures 2A and 2B). The specificity of AAV-SST-mCherry in labeling SST positive neurons has been proved in a previous published article.[32] Electrophysiological recordings from CeL slices revealed that the frequency of evoked firing in current-clamped CeL^{SOM} neurons was markedly elevated in FC mice compared with control mice (***$p = 0.0002$, two-way ANOVA test, Figure 2C). Consistent with previous reports, FC induced an enhancement of excitatory synaptic transmission onto CeL^{SOM} neurons, as indicated by an increase in the frequency and amplitude of mEPSCs recorded from CeL^{SOM} neurons (For frequency, ****$p < 0.0001$, two-sided unpaired *t*-test; for amplitude, **$p = 0.002$, two-sided unpaired *t*-test, Figures 2D and 2E).

Furthermore, we performed a loss-of-function experiment to confirm the importance of CeL^{SOM} neurons in fear memory acquisition at the behavioral level. We injected the CeL with a mixture of AAV-fSST-Cre and AAV-DIO-eNpHR3.0 (Figures 2F and 2G), implanted an optical fiber into the CeL. Optogenetic inhibition of CeL^{SOM} neurons during the FC session significantly impaired fear memory learning, as indicated by reduced freezing to the third CS, as well as the expression of contextual and cued fear memory during the fear memory test (For the training period, $p = 0.277$, two-way ANOVA test, Figure 2H; For the contextual test, **$p = 0.0097$, two-sided unpaired *t*-test; Figure 2I; For the cued test, *$p = 0.011$, two-way ANOVA test; Figure 2J). In addition, infusing the selective NMDA (N-Methyl-D-aspartic acid) receptor antagonist

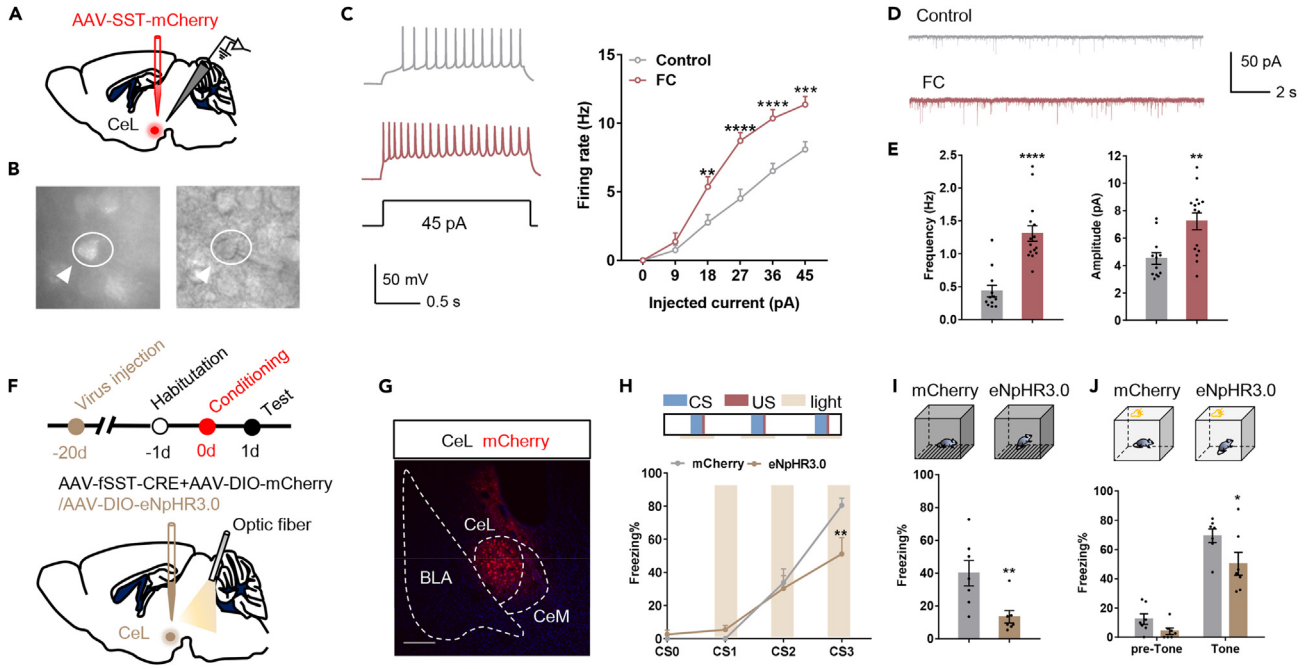

Figure 2. Enhanced activity of CeL SOM neurons after fear conditioning

(A) Schematic showing virus microinjection.

(B) Electrophysiological recording of virus-labeled SOM$^+$ neurons in the CeL.

(C) Sample traces (left) and statistical data (right) of firing rates recorded from CeL-SOM$^+$ neurons (two-way ANOVA, group: $F_{(1,24)} = 18.67$, ***$p = 0.0002$; Bonferroni's post hoc test, Control versus FC at 18 pA, **$p = 0.007$; Control versus FC at 27 pA, ****$p < 0.0001$; Control versus FC at 36 pA, ****$p < 0.0001$; Control versus FC at 45 pA, ***$p = 0.0003$; $n = 12$ cells from 3 mice for Control, $n = 14$ cells from 3 mice for FC).

(D) Representative mEPSC traces recorded from mCherry-labeled CeL-SOM$^+$ neurons.

(E) Compared with the Control group, the mEPSC frequency (left) and amplitude (right) of CeL-SOM$^+$ neurons in the FC group showed a marked increase (two-sided unpaired t-test, For frequency, $t_{(1/25)} = 3.458$, ****$p < 0.0001$; For amplitude, $t_{(1/25)} = 5.708$, **$p = 0.002$. $n = 12$ cells from 3 mice for Control, $n = 15$ cells from 3 mice for FC).

(F) Time course (left) and schematic (right) of bilateral CeL injection of eNpHR and mCherry viruses with insertion of optic fibers above the CeL.

(G) Representative images showing the expression of mCherry-labeled CeL-SOM$^+$ neurons and cannula placement in the CeL. Scale bar, 200 μm.

(H) Top, Schematic of the optogenetic protocol. Bottom, Optogenetic silencing of CeL-SOM$^+$ neurons induced a significant decrease in the freezing levels at the end of fear conditioning (two-way ANOVA, group: $F_{(1,12)} = 1.298$, $p = 0.2769$; time: $F_{(3,36)} = 80.01$, ****$p < 0.0001$; interaction: $F_{(3,36)} = 5.444$, **$p = 0.0034$; Bonferroni's post hoc test, freezing for eNpHR3.0 versus mCherry at CS3, **$p = 0.0025$; $n = 7$ mice).

(I and J) Mice that had undergone optogenetic inhibition of CeL-SOM$^+$ neurons showed impaired fear memory recall in the contextual (I, two-sided unpaired t-test, $t_{(1/12)} = 3.07$, **$p = 0.0097$, $n = 7$ mice) and cued (J, two-way ANOVA, group: $F_{(1,12)} = 9.072$, *$p = 0.0108$; time: $F_{(1,12)} = 90$, ****$p < 0.0001$; interaction: $F_{(1,12)} = 0.999$, $p = 0.337$; Bonferroni's post hoc test, freezing for eNpHR3.0 versus mCherry during tone presentation, *$p = 0.0248$; $n = 7$ mice for each group) fear memory tests. All of the data are presented as mean ± SEM. *$p < 0.05$, **$p < 0.01$, ***$p < 0.001$, ****$p < 0.0001$.

MK-801 into the CeL impaired conditioned fear memory learning in FC mice (Figure S2A; For the training period, ****$p < 0.0001$, two-way ANOVA test; Figure S2B; For the contextual test, **$p = 0.008$, two-sided unpaired t-test; Figure S2C; For the cued test, ****$p < 0.0001$, two-way ANOVA test; Figure S2D). Similar effects were obtained with intra-CeL infusions of the non-NMDA receptor antagonist NBQX (2,3-dihydroxy-6-nitro-7-sulfamoyl benzo(F)quinoxaline) in FC mice (Figure S2E; for the training period, ****$p < 0.0001$, two-way ANOVA test; Figure S2F; For the contextual test, **$p = 0.0018$, two-sided unpaired t-test; Figure S2G; For the cued test, ****$p < 0.0001$, two-way ANOVA test; Figure S2H). Combining the behavioral results with the electrophysiological changes observed in CeL^{SOM} neurons, our results support the hypothesis that enhanced excitatory input into the CeL may facilitate the acquisition of conditioned fear memories in mice.

Neuroanatomical identification of the LPB^{Glu}→CeL^{SOM} and PVT^{Glu}→CeL^{SOM} pathways

Given that increased excitatory transmission onto the CeL is necessary for conditioned fear memory acquisition in FC mice, we concentrated our attention on elucidating the upstream networks that drive and regulate CeL neuronal activity. To label the upstream cells that project directly onto CeL neurons, we injected Lumafluor retrobeads into the CeL for retrograde tracing (Figure 3A). Brain-wide analyses of Lumafluor$^+$ cells identified the bed nucleus of the stria terminalis (BNST), the PVT, the ventral tegmental area (VTA), and the LPB as the major input sources onto CeL neurons (Figure 3B). To explore whether these upstream nuclei are involved in fear memory acquisition, we examined changes in activity in these nuclei after FC by measuring c-Fos expression, a marker of neuronal activity. The expression of c-Fos was increased

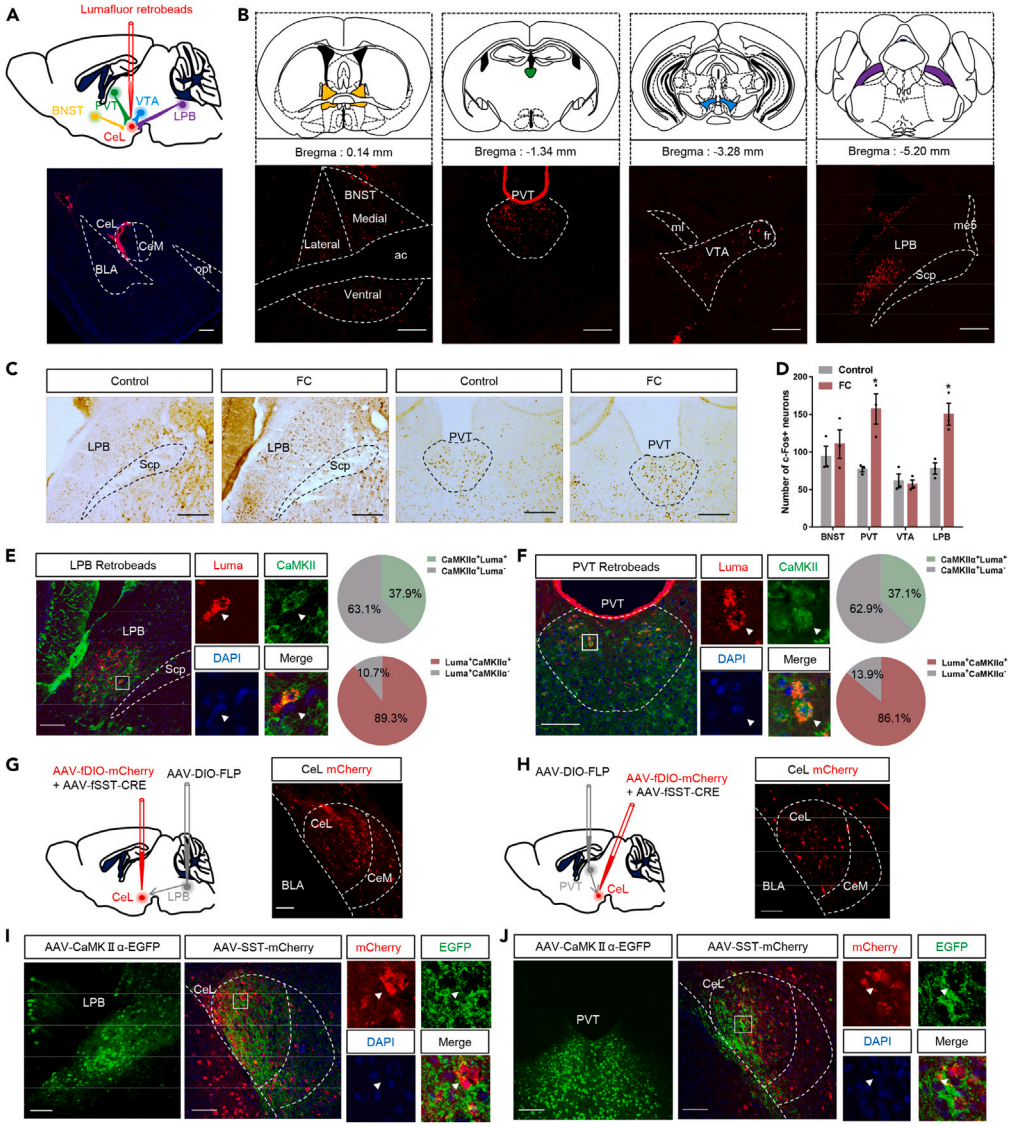

Figure 3. Neuroanatomical identification of genetically defined LPB^{Glu}→CeL^{SOM} and PVT^{Glu}→CeL^{SOM} pathways

(A) Top, Schematic of bilateral CeL injection of Lumafluor retrobeads to trace the nuclei upstream of the CeL. Bottom, A representative image showing the expression of Lumafluor retrobeads in CeL coronal section. Scale bar, 200 μm.

(B) Top, Schema of coronal sections showed the specific locations of the BNST (orange), PVT (green), VTA (blue) and LPB (purple) at four sagittal locations (bregma 0.14, −1.34, −3.28, and −5.20 mm). BNST, bed nucleus of stria terminalis; VTA, ventral tegmental area. Bottom, Representative images of upstream Lumafluor$^+$ neurons providing direct inputs to the CeL. Scale bar, 200 μm.

(C and D) Representative histological examples and quantification of c-Fos$^+$ cells in the identified upstream nuclei of the CeL after fear conditioning (two-sided unpaired *t*-test, BNST: $t_{(1/4)} = 0.713$, $p = 0.516$; PVT: $t_{(1/4)} = 3.93$, $^*p = 0.017$; VTA: $t_{(1/4)} = 0.434$, $p = 0.687$; LPB: $t_{(1/4)} = 4.372$, $^*p = 0.012$, $n = 3$ mice).

(E and F) Left, Representative images of Lumafluor-labeled neurons within the LPB (E) or PVT (F) co-localized with the glutamate marker CaMKIIα, together with high-magnification images from the selected area. Scale bar, 100 μm. Right, Pie charts showing the percentage of CaMKIIα-positive neurons that were co-labeled with Lumafluor and Lumafluor-labeled neurons that were co-labeled by CaMKIIα.

(G and H) Left, Schematic of the Cre-dependent anterograde virus tracing strategy. Right, Immunofluorescence images showing mCherry-labeled neurons within the CeL traced from the LPB (G) or PVT (H). Scale bar, 100 μm.

(I and J) Left, Immunofluorescence images showing EGFP-labeled neurons within the LPB (I) or PVT (J). Scale bar, 100 μm. Middle, Representative images showing that the EGFP-labeled glutamatergic axon terminals from the LPB and PVT made close appositions onto the mCherry-labeled SOM$^+$ cell bodies in the CeL. Scale bar, 100 μm. Right, magnified images from the selected area of the middle images. All of the data are presented as mean ± SEM. $^*p < 0.05$.

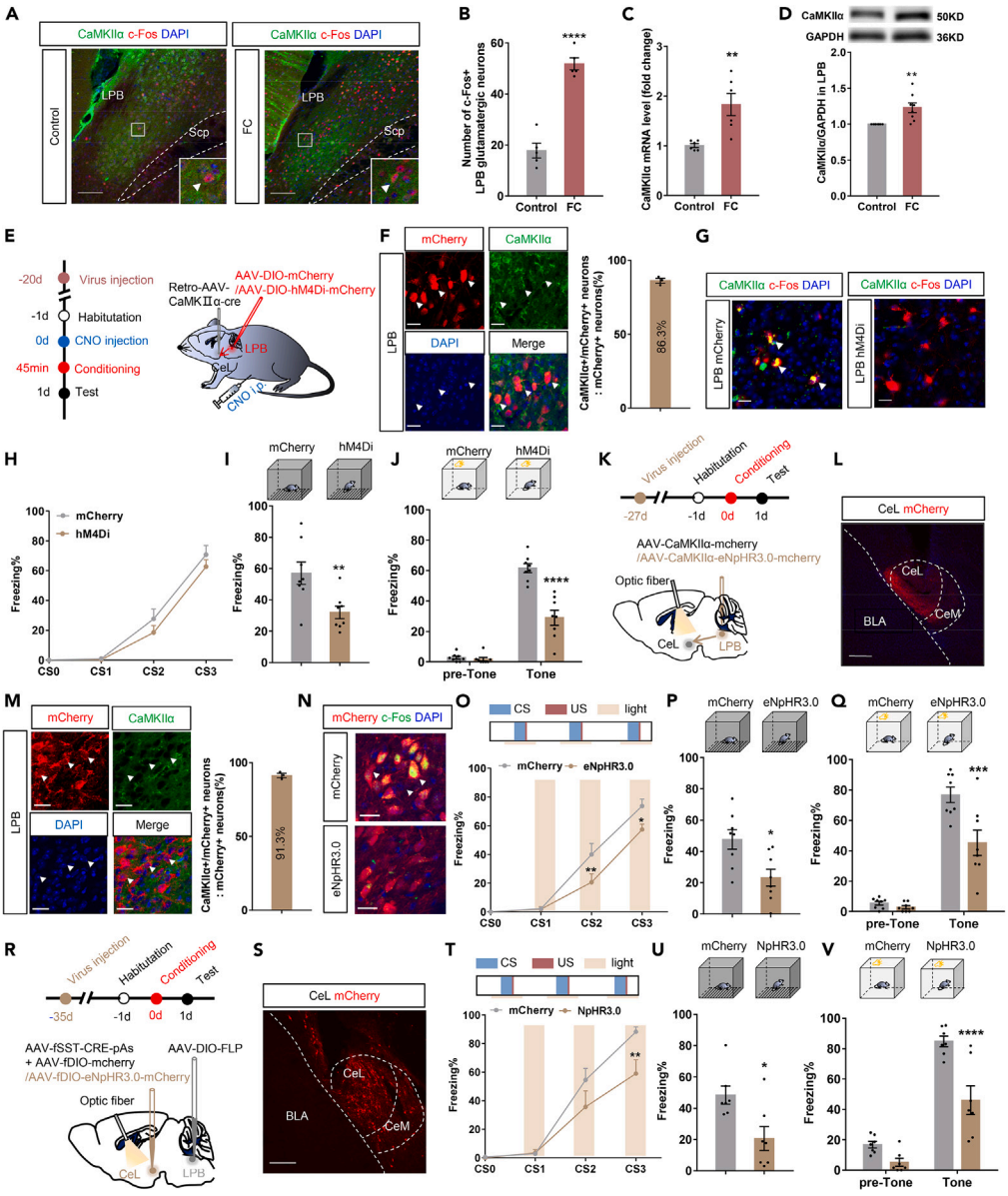

Figure 4. Neural projections from the LPB to the CeL mediate fear memory acquisition

(A and B) Immunofluorescence images (A) and percentage (B) of c-Fos^{+} neurons in the LPB co-labeled with CaMKIIα after fear conditioning (two-sided unpaired *t*-test, $t_{(1/8)} = 9.126$, $^{****}p < 0.0001$, $n = 5$ mice for each group). Scale bar, 100 μm.

(C and D) CaMKIIα mRNA (C, two-sided unpaired *t*-test, $t_{(1/10)} = 3.635$, $^{**}p = 0.0046$, $n = 6$ mice) and protein (D, two-sided unpaired *t*-test, $t_{(1/14)} = 3.426$, $^{**}p = 0.0041$, $n = 8$ mice for each group) levels in the LPB were significantly greater in FC mice than control mice.

(E) Timeline (left) and schematic (right) of chemogenetic inhibition of the CeL-projecting LPB glutamatergic neurons.

(F) Representative images of mCherry-labeled neurons in LPB co-localized with CaMKIIα (left), and the proportion of co-labeled neurons relative to the total number of mCherry-labeled neurons (right). Scale bar, 20 μm.

(G) Immunofluorescence showing that intra-LPB injections of the hM4Di-mCherry virus induced a decrease in c-Fos co-expression after CNO administration, relative to the control mCherry group. Scale bar, 20 μm.

(H) Mice that received chemogenetic inhibition of CeL-projecting LPB glutamatergic neurons had similar freezing levels throughout the fear conditioning session as the mCherry mice (two-way ANOVA, group: $F_{(1,14)} = 1.529$, $p = 0.2366$; time: $F_{(3,42)} = 155.7$, $^{****}p < 0.0001$; interaction: $F_{(3,42)} = 0.8946$, $p = 0.4519$; $n = 8$ mice).

(I and J) Chemogenetic inhibition of the CeL-projecting LPB glutamatergic neurons induced a decrease in freezing levels during the contextual (I, two-sided unpaired *t*-test, $t_{(1/14)} = 3.063$, $^{**}p = 0.0084$, $n = 8$ mice) and cued (J, two-way ANOVA, group: $F_{(1,14)} = 27.3$, $^{***}p = 0.0001$; time: $F_{(1,14)} = 268.8$, $^{****}p < 0.0001$; interaction: $F_{(1,14)} = 36.39$, $^{****}p < 0.0001$; Bonferroni's post hoc test, freezing for hM4Di versus mCherry during Tone presentation, $^{****}p < 0.0001$; $n = 8$ mice) fear memory tests.

(K) Time course (top) and paradigm (bottom) for the optogenetic inhibition of LPB glutamatergic nerve terminals in the CeL.

Figure 4. *Continued*

(L) Representative histological images showing the expression of mCherry$^+$ fibers in the CeL and optical fibers inserted above the target area. Scale bar, 200 μm.

(M) Representative images of mCherry-labeled neurons in the LPB co-localized with CaMKIIα (left), and the proportion of co-labeled neurons relative to the total number of mCherry-labeled neurons (right). Scale bar, 20 μm.

(N) Optogenetic inhibition of glutamatergic neurons dramatically reduced the Fos-like immunoreactivity within the LPB. Scale bar, 20 μm.

(O) Top, Schematic of the optogenetic protocol. Bottom, mice that underwent optogenetic inhibition of LPB glutamatergic terminals in the CeL exhibited decreased freezing levels during the second and third CS presentation during fear conditioning compared with the mCherry mice (two-way ANOVA, group: $F_{(1,14)} = 5.682$, $^*p = 0.0318$; time: $F_{(3,42)} = 139.1$, $^{****}p < 0.0001$; interaction: $F_{(3,42)} = 3.91$, $^*p = 0.015$; Bonferroni's post hoc test, freezing for eNphR3.0 versus mCherry at CS2, $^{**}p = 0.0069$; freezing for eNphR3.0 versus mCherry at CS3, $^*p = 0.0297$; $n = 8$ mice).

(P and Q) Optogenetic inhibition of LPB glutamatergic terminals in the CeL caused a decrease in freezing levels in the contextual (P, two-sided unpaired *t*-test, $t_{(1/14)} = 2.956$, $^*p = 0.0104$, $n = 8$ mice) and cued (Q, two-way ANOVA, group: $F_{(1,14)} = 10.02$, $^{**}p = 0.0069$; time: $F_{(1,14)} = 161.8$, $^{****}p < 0.0001$; interaction: $F_{(1,14)} = 10.41$, $^{**}p = 0.0061$; Bonferroni's post hoc test, freezing for eNphR3.0 versus mCherry during Tone presentation, $^{***}p = 0.0002$; $n = 8$ mice) fear memory tests.

(R) Schematic for the optogenetic inhibition of CeL^{SOM} neurons innervated by LPB terminals.

(S) Representative histological images showing the expression of mCherry-labeled SOM+ neurons in the CeL and optical fiber insertion above the target area. Scale bar, 200 μm.

(T) Top, Schematic of optogenetic protocol. Bottom, Mice that underwent optogenetic inhibition of CeL^{SOM} neurons innervated by LPB exhibited decreased freezing levels at the end of fear conditioning (two-way ANOVA, group: $F_{(1,12)} = 4.551$, $p = 0.0542$; time: $F_{(3,36)} = 84.47$, $^{****}p < 0.0001$; interaction: $F_{(3,36)} = 3.602$, $^*p = 0.0225$; Bonferroni's post hoc test, freezing for NphR3.0 versus mCherry at CS3, $^{**}p = 0.006$; $n = 7$ mice).

(U and V) Optogenetic inhibition of CeL ^{SOM} neurons innervated by LPB terminals caused a decrease in freezing levels in the contextual (U, two-sided unpaired *t*-test, $t_{(1/12)} = 2.91$, $^*p = 0.0131$, $n = 7$ mice) and cued (V, two-way ANOVA, group: $F_{(1,12)} = 16.72$, $^{**}p = 0.0015$; time: $F_{(1,12)} = 162.7$, $^{****}p < 0.0001$; interaction: $F_{(1,12)} = 10.02$, $^{**}p = 0.0081$; Bonferroni's post hoc test, freezing for NphR3.0 versus mCherry during Tone presentation, $^{****}p < 0.0001$; $n = 7$ mice) fear memory tests. All of the data are presented as mean ± SEM. $^*p < 0.05$, $^{**}p < 0.01$, $^{***}p < 0.001$, $^{****}p < 0.0001$.

in the PVT and LPB in FC mice, whereas no alterations were observed in the BNST or VTA (Figure 3C; For BNST, $p = 0.516$, two-sided unpaired *t*-test; For PVT, $^*p = 0.017$, two-sided unpaired *t*-test; For VTA, $p = 0.687$, two-sided unpaired *t*-test; For LPB, $^*p = 0.012$, two-sided unpaired *t*-test; Figure 3D). These data confirm that the LPB and PVT are the upstream structures that project directly to CeL, seemingly playing an important role in driving freezing behavior. Thus, we determined to elucidate the anatomical connections from these two upstream nuclei to the CeL in more detail.

We first characterized the LPB→CeL and PVT→CeL organization by combining the Lumafluor retrograde tracing with immunofluorescence staining. The Lumafluor$^+$ cells in the LPB and PVT that project to the CeL predominantly colocalized with antibodies for CaMKII (specific to glutamatergic neurons), suggesting that glutamatergic neurons in the LPB and PVT constitute the major neuronal type that projects to the CeL (Figures 3E and 3F). To specifically label the downstream neuronal type of the LPB→CeL and PVT→CeL pathway, we used a cell-type-specific anterograde monosynaptic tracing system. As follows, we injected a Cre-dependent virus (AAV-DIO-FLP) into the LPB or the PVT and a mixture of AAV-fDIO-mCherry and AAV-fSST-CRE into the CeL (Figures 3G and 3H, left). Four weeks later, mCherry-positive CeL^{SOM} neurons were observed in the CeL (Figures 3G and 3H, right). For further confirmation of the LPB→CeL and PVT→CeL projections, we infused AAV-CaMKIIα-EGFP into the LPB or PVT and AAV-SST-mCherry into the CeL to examine the relationship between LPB or PVT glutamatergic nerve terminals and SOM$^+$ neuronal cell bodies within the CeL (Figures 3I and 3J, left). Close appositions were observed between the LPB or PVT glutamatergic nerve terminals and the mCherry-labeled SOM$^+$ neuronal cell bodies (Figures 3I and 3J, right), indicating that the SOM$^+$ neurons in the CeL receive glutamatergic innervation from the LPB and PVT. Taken together, these results suggested the existence of LPB^{Glu}→CeL^{SOM} and PVT^{Glu}→CeL^{SOM} projections. These findings prompted us to propose the hypothesis that the LPB^{Glu}→CeL^{SOM} and PVT^{Glu}→CeL^{SOM} pathways are involved in fear memory acquisition.

Essential role of the LPB^{Glu}→CeL^{SOM} pathway in acquisition of fear memories

We predicted that the increased excitability of CeL^{SOM} neurons after FC may be due to an increase in LPB^{Glu} activity. To test this, we measured c-Fos expression in the LPB after FC. We observed many c-Fos$^+$ glutamatergic neurons in the LPB in the FC group, in contrast to the scarcity of c-Fos$^+$ glutamatergic neurons in the control group (Figure 4A; $^{****}p < 0.0001$, two-sided unpaired *t*-test; Figure 4B). We also used western blots and Quantitative reverse transcription polymerase chain reaction (RT-qPCR) to detect the expression of CaMKIIα, an important serine/threonine protein kinase phosphorylates synapsin I and AMPAR to promote the release of excitatory neurotransmitters, thus playing an important role in synaptic plasticity.[33–35] The elevated CaMKIIα mRNA and protein levels implied enhanced neuronal activity (For mRNA, $^{**}p = 0.0046$, two-sided unpaired *t*-test, Figure 4C; For protein, $^{**}p = 0.0041$, two-sided unpaired *t*-test; Figure 4D). These data demonstrate that LPB^{Glu} neurons are activated during FC, when conditioned fear memories are acquired.

To explore whether the hyperactivity of CeL-projecting LPB^{Glu} neurons is necessary for the acquisition of conditioned fear memories, we manipulated this group of glutamatergic neurons with a chemogenetic approach. Retro-AAV-CaMKIIα-Cre was injected into the CeL and a Cre-dependent chemogenetic vector or control (AAV-DIO-hM4Di-mCherry or AAV-DIO-mCherry) was injected into the LPB to enable chemogenetic inhibition of CeL-projecting glutamatergic neurons in the LPB; Figure 4E illustrates the timeline of the experiment. Immunofluorescence indicated that mCherry$^+$ neurons in the LPB were predominantly co-localized with glutamatergic neurons, verifying the specificity of the injected AAV viruses (Figure 4F). We also confirmed that CNO injection indeed decreased c-Fos expression in CeL-projecting glutamatergic neurons in the hM4Di group (Figure 4G; $^{**}p = 0.0016$, two-sided unpaired *t*-test; Figure S1B). In the behavioral tests, chemogenetic inhibition of CeL-projecting LPB^{Glu} neurons during FC impaired contextual and cued fear memory acquisition (For the contextual test,

**$p = 0.0084$, two-sided unpaired *t*-test, Figure 4I; For the cued test, ****$p < 0.0001$, two-way ANOVA test; Figure 4J), although no significant effects on freezing were observed during the FC session ($p = 0.237$, two-way ANOVA test, Figure 4H).

To transiently manipulate the pathway, we used optogenetic techniques to inhibit LPB^{Glu} terminals in the CeL. AAV-CaMKIIα-eNpHR3.0-mCherry was injected into the LPB and optical fibers were inserted into the CeL (Figures 4K and S3A). The specificity and efficacy of the injected virus were confirmed by immunohistochemistry (Figures 4M and 4N). As a result, eNpHR3.0-mCherry was expressed on both the somata and terminals of glutamatergic neurons (Figures 4L and 4M). Optogenetic inhibition of the glutamatergic terminals in the LPB→CeL pathway with yellow light markedly decreased freezing during FC (*$p = 0.032$, two-way ANOVA test, Figure 4O), as well as in the contextual and cued fear memory tests (For the contextual test, *$p = 0.010$, two-sided unpaired *t*-test, Figure 4P; For the cued test, ***$p = 0.0069$, two-way ANOVA test; Figure 4Q). To rule out the possibility that functional inactivation of the LPB pathway to the CeL may have affected the nociceptive threshold for the foot shock, we examined whether inhibiting the LPB^{Glu} terminals in the CeL affects nociceptive sensitivity, as measured with von Frey filaments. No significant difference was observed between the eNpHR and control groups, suggesting that the decreased freezing observed in the fear memory test was due to weakened fear memory acquisition rather than reduced nociceptive sensitivity ($p = 0.4558$, two-way ANOVA test, Figure S3B). Furthermore, studies have demonstrated that fear learning depends on cognitive capabilities, including working memory (WM), and individuals with low WM abilities tend to exhibit more negative intrusive thoughts.[36,37] The interplay between WM and emotions implies that individual differences in WM might also have an effect on the acquisition of fear.[36] Therefore, we investigated the role of the LPB^{Glu}→CeL^{SOM} pathway in spatial WM in FC model mice by inhibiting the pathway during the Y-maze test. Nevertheless, we found that there was no significant difference of the time in the novel arm between mCherry and hM4Di group ($p = 0.48$, two-sided unpaired *t*-test, Figure S3D).

In order to specifically inhibit downstream CeL^{SOM} neurons that are innervated by the LPB, we injected a Cre-dependent anterograde monosynaptic virus (AAV-DIO-FLP) into the LPB and a mixture of AAV-fDIO-eNpHR3.0-mCherry (or AAV-fDIO-mCherry) and AAV-fSST-CRE into the CeL (Figure 4R). Accordingly, mCherry-labeled SOM^+ neurons were abundantly distributed in the CeL (Figure 4S). Optogenetic inhibition of these CeL^{SOM} neurons innervated by the LPB impaired both conditioned fear memory learning and acquisition, as evidenced by decreased freezing during FC and in the subsequent fear memory tests (for the training period, $p = 0.054$, two-way ANOVA test, Figure 4T; For the contextual test, *$p = 0.013$, two-sided unpaired *t*-test; Figure 4U; For the cued test, **$p = 0.0015$, two-way ANOVA test; Figure 4V). From these results, we can conclude that activation of the LPB^{Glu}→CeL^{SOM} pathway is necessary for the acquisition of conditioned fear memories.

Specific regulation of fear memory expression by the PVT^{Glu}→CeL^{SOM} pathway

Previous studies have shown that increased activity in PVT neurons is responsible for fear-like behaviors and that elevated excitability in CeL-projecting PVT neurons facilitates anxiety, both of which support the idea that dysfunction in the PVT→CeL pathway may account for fear memory acquisition and expression.[38,39] To test the importance of the PVT^{Glu}→CeL^{SOM} projection in mediating freezing behavior after FC, we first examined the activity of PVT^{Glu} neurons. Consistent with previous reports,[13] we observed increased c-Fos expression in glutamatergic PVT neurons after FC (Figure 5A; *$p = 0.016$, two-sided unpaired *t*-test; Figure 5B). Similarly, with western blots and RT-qPCR, we observed elevated CaMKIIα mRNA and protein levels after FC, suggesting an increase in the synthesis and release of excitatory neurotransmitters by PVT^{Glu} neurons in FC mice (For mRNA, **$p = 0.0032$, two-sided unpaired *t*-test, Figure 5C; For protein, ***$p = 0.0004$, two-sided unpaired *t*-test; Figure 5D).

To ascertain whether the enhanced excitatory input from the PVT to the CeL is implicated in the acquisition of fear memories, we used a similar chemogenetic approach as before to specifically manipulate CeL-projecting PVT glutamatergic neurons (Figure 5E). Immunofluorescence staining in brain sections expressing $mCherry^+$ cells confirmed that the majority of infected PVT neurons were glutamatergic (Figure 5F). Behavioral results indicated that chemogenetic inhibition of the CeL-projecting PVT glutamatergic neurons impaired cued fear memory acquisition (*$p = 0.011$, two-way ANOVA test, Figure 5I), although no effects were observed during the FC session or in the contextual fear memory test (for the training period, $p = 0.509$, two-way ANOVA test, Figure 5G; for the contextual test, $p = 0.178$, two-sided unpaired *t*-test; Figure 5H). Hyper-excitability of PVT neurons has been implicated in the pathogenesis of mechanical hyperalgesia,[40] raising the possibility that decreased nociceptive sensitivity may underlie the effects of pathway inhibition on freezing behaviors. However, chemogenetic inhibition of the PVT^{Glu}→CeL pathway did not alter mechanical pain thresholds, as measured with von Frey filaments ($p = 0.5633$, two-way ANOVA test, Figure S3C).

We next used optogenetics to further test the role of the PVT^{Glu}→CeL pathway in the acquisition of conditioned fear memories (Figure 5J). The specificity of the injected viruses was verified via CaMKIIα staining (Figure 5K). However, behavioral tests revealed that optogenetic inhibition of eNpHR-containing PVT^{Glu} terminals in the CeL had no significant effect on fear memory acquisition: freezing levels both during the FC and in the fear memory tests were equivalent in the eNpHR and control groups (for the training period, $p = 0.592$, two-way ANOVA test, Figure 5L; For the contextual test, $p = 0.738$, two-sided unpaired *t*-test; Figure 5M; For the cued test, $p = 0.210$, two-way ANOVA test; Figure 5N). Given the differences observed in the behavioral tests with chemogenetic and optogenetic manipulations, we speculate that the PVT^{Glu}→CeL pathway may tend to mediate the expression of fear memories rather than fear memory acquisition in FC mice. To summarize, our data suggest a crucial role for the LPB^{Glu}→CeL^{SOM} pathway in fear memory acquisition, but not for the PVT^{Glu}→CeL pathway.

CB1Rs are selectively located at LPB^{Glu}→CeL^{SOM} terminals and regulate synaptic activity

Given that elevated activity in the LPB^{Glu}→CeL^{SOM} pathway underlies the acquisition of fear memories, we wondered to investigate the molecular mechanism mediating such alterations in the circuit excitability. We therefore hypothesized that CB1R-mediated feedforward

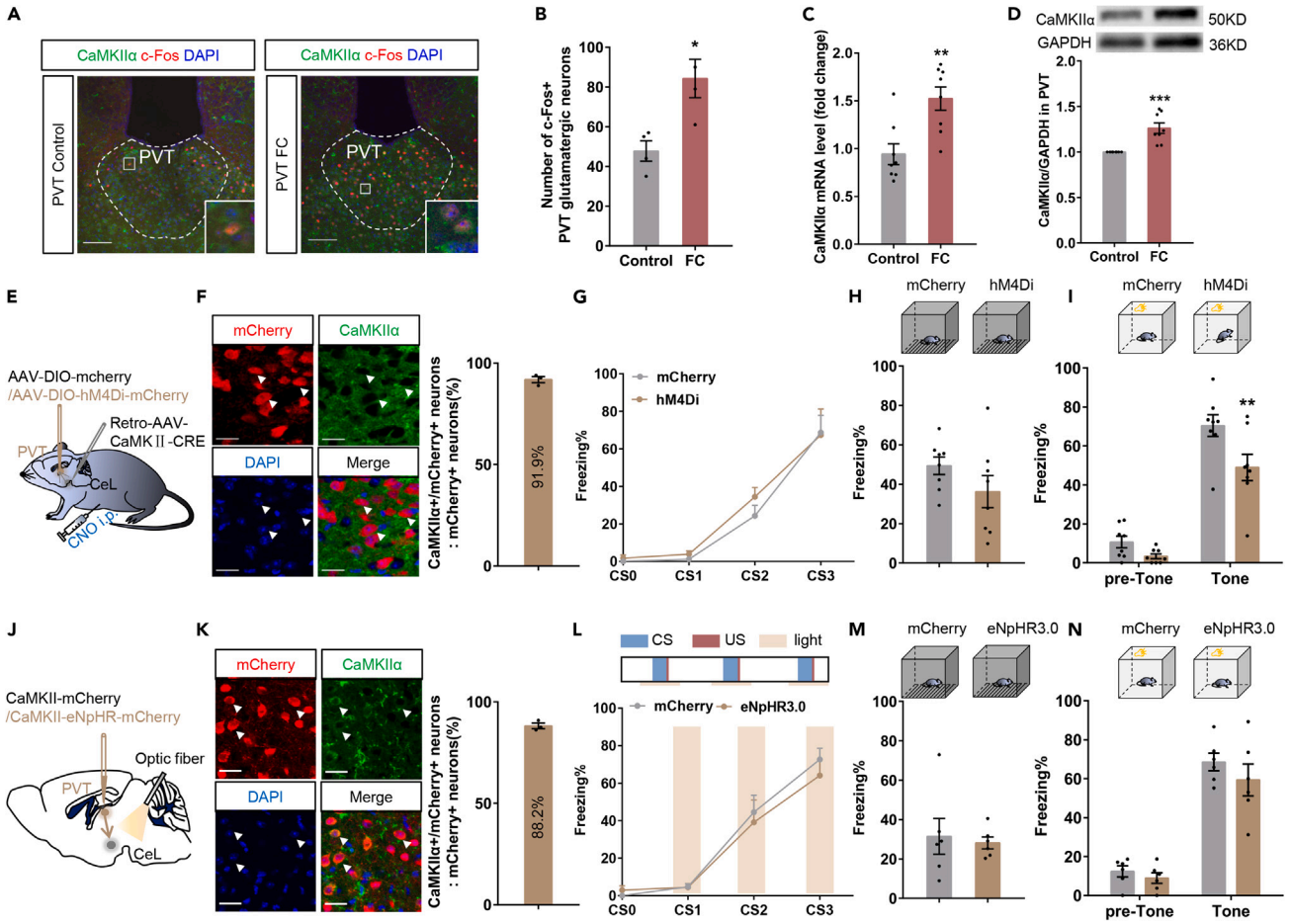

Figure 5. Specific modulation of fear memory expression by CeL-projecting PVT glutamatergic neurons

(A and B) Immunofluorescence images (A) and percentage (B) of c-Fos$^+$ neurons in the PVT co-labeled with CaMKIIα after fear conditioning (two-sided unpaired *t*-test, $t_{(1/6)} = 3.34$, $^*p = 0.016$, $n = 4$ mice). Scale bar, 100 μm.

(C and D) CaMKIIα mRNA (C, two-sided unpaired *t*-test, $t_{(1/14)} = 3.551$, $^{**}p = 0.0032$, $n = 8$ mice) and protein (D, two-sided unpaired *t*-test, $t_{(1/14)} = 4.564$, $^{***}p = 0.0004$, $n = 8$ mice) expression in the PVT were significantly upregulated in FC mice versus control mice.

(E) Experiment design for chemogenetic inhibition of the CeL-projecting PVT glutamatergic neurons.

(F) Example images of CaMKIIα$^+$ neurons in the PVT infected with the hM4Di-mCherry or mCherry virus (left), and the proportion of co-labeled neurons relative to the total number of mCherry-labeled neurons (right). Scale bar, 20 μm.

(G) Mice that received chemogenetic inhibition of CeL-projecting PVT glutamatergic neurons had similar freezing levels throughout the fear conditioning session as the mCherry mice (two-way ANOVA, group: $F_{(1,14)} = 0.4593$, $p = 0.509$; time: $F_{(3,42)} = 48.36$, $^{****}p < 0.0001$; interaction: $F_{(3,42)} = 0.2886$, $p = 0.833$; $n = 8$ mice).

(H) Chemogenetic inhibition of the CeL-projecting PVT glutamatergic neurons did not affect the freezing levels in the contextual fear memory test (two-sided unpaired *t*-test, $t_{(1/14)} = 1.42$, $p = 0.178$, $n = 8$ mice).

(I) Chemogenetic inhibition of the CeL-projecting PVT glutamatergic neurons induced a significant decrease in freezing levels during tone presentation in the cued fear memory test (two-way ANOVA, group: $F_{(1,14)} = 8.579$, $^*p = 0.011$; time: $F_{(1,14)} = 142$, $^{****}p < 0.0001$; interaction: $F_{(1,14)} = 2.553$, $p = 0.1324$; Bonferroni's post hoc test, freezing for hM4Di versus mCherry during Tone presentation, $^{**}p = 0.0061$; $n = 8$ mice).

(J) Schematic paradigm (right) for optogenetic inhibition of PVT glutamatergic terminals in the CeL.

(K) Example images of CaMKIIα$^+$ neurons in the PVT infected with the eNphR-mCherry or mCherry virus (left), and the proportion of co-labeled neurons relative to the total number of mCherry-labeled neurons (right). Scale bar, 20 μm.

(L) Top, Schematic of the optogenetic protocol. Bottom, Mice that underwent optogenetic inhibition of PVT glutamatergic terminals in the CeL exhibited similar freezing levels throughout the fear conditioning session as the mCherry mice (two-way ANOVA, group: $F_{(1,10)} = 0.3063$, $p = 0.5921$; time: $F_{(3,30)} = 50.69$, $^{****}p < 0.0001$; interaction: $F_{(3,30)} = 0.3257$, $p = 0.8068$; $n = 6$ mice).

(M and N) Optogenetic inhibition of PVT glutamatergic terminals in the CeL did not affect the freezing levels in the contextual (M, two-sided unpaired *t*-test, $t_{(1/10)} = 0.344$, $p = 0.738$, $n = 6$ mice) or cued (N, two-way ANOVA, group: $F_{(1,10)} = 1.794$, $p = 0.2101$; time: $F_{(1,10)} = 94.74$, $^{****}p < 0.01$; interaction: $F_{(1,10)} = 0.2846$, $p = 0.6053$; $n = 6$ mice) fear memory tests. All of the data are presented as mean ± SEM. $^*p < 0.05$, $^{**}p < 0.01$, $^{***}p < 0.001$.

inhibition may modulate synaptic transmission within the circuit. To confirm the expression of CB1Rs in CeL-projecting LPB^{Glu} neurons, we selectively labeled LPB^{Glu} neurons with intra-LPB injections of AAV-CaMKIIα-mCherry (Figure 6A) and then costained sections for CB1R in the CeL. We found that 77.4% of CB1R expression in the CeL was at LPB glutamatergic terminals (Figure 6B). In the same way, we detected that 59.9% of CB1R expression in the CeL was at PVT glutamatergic terminals (Figures 6C and 6D). *In situ* hybridization showed that 92.3% of CB1R mRNA-positive neurons in the LPB were also positive for CaMKIIα mRNA and that 58.9% of CaMKIIα mRNA-positive neurons were also positive for CB1R mRNA (Figures 6I and 6J).

Because of the enhanced synaptic transmission in the $LPB^{Glu} \rightarrow CeL^{SOM}$ pathway in FC mice and the role of CB1Rs in regulating synaptic transmission, we predicted that the expression of CB1Rs in this pathway would be associated with fear memory acquisition. Consistent with this, expression of the total CB1R protein in the CeL and expression of CB1R mRNA in the LPB was significantly greater in FC mice than control mice (for protein, $^{**}p = 0.0066$, two-sided unpaired *t*-test, Figure 6E; For mRNA, $^{**}p = 0.0018$, two-sided unpaired *t*-test; Figure 6F). In addition, we found that the mRNA expression level of fatty acid amide hydrolase (FAAH), an endogenous cannabinoid hydrolase, exhibited a marked increase in the CeL of FC mice, which suggests a potential role of endogenous cannabinoids in regulating synaptic transmission in the CeL ($^{**}p = 0.005$, two-sided unpaired *t*-test, Figure 6G). Moreover, there was no difference in CB1R mRNA expression in the PVT between the FC and control groups, further confirming the lack of FC-induced CB1R modulation of synaptic transmission in the PVT→CeL pathway ($p = 0.7783$, two-sided unpaired *t*-test, Figure 6H). These results suggest that expression of CB1Rs in the $LPB^{Glu} \rightarrow CeL^{SOM}$ pathway plays a critical role in synaptic transmission, and that the FC-induced increase in CB1R expression may exert a regulating effect on the acquisition of conditioned fear memories.

CB1Rs in the $LPB^{Glu} \rightarrow CeL^{SOM}$ pathway participate in cannabinoid-induced impairments in fear memory acquisition

Next, we used slice electrophysiology to verify the function of CB1Rs in the $LPB^{Glu} \rightarrow CeL^{SOM}$ pathway (Figure 7A). In agreement with previous studies,[41,42] application of the CB1R agonist WIN55,212-2 dramatically decreased the amplitude of evoked EPSCs (eEPSCs) recorded from CeL^{SOM} neurons, whereas inhibition of CB1R by the antagonist AM251 markedly increased the amplitude of eEPSCs (Figure 7B; $^{****}p < 0.0001$, one-way ANOVA test; Figure 7C). This indicates that CB1Rs located at the $LPB^{Glu} \rightarrow CeL^{SOM}$ terminals can regulate synaptic transmission in this pathway.

To test the causal link between CB1R function and fear memory acquisition, we injected the cannabinoid agonist WIN55,212–2 into the CeL (Figure 7D). Pharmacological activation of CB1Rs did not alter freezing levels during FC ($p = 0.5988$, two-way ANOVA test, Figure 7E), but did impair fear memory acquisition, as shown by decreased freezing in the contextual and cued fear memory tests (for the contextual test, $^{***}p = 0.0004$, one-way ANOVA test, Figure 7F; For the cued test, $p = 0.0777$, two-way ANOVA test; Figure 7G). Furthermore, the effects of WIN55,212–2 on fear memory acquisition could be partly reversed by co-administration of the CB1R antagonist AM251 (Figures 7F and 7G), supported the idea that WIN55,212–2-induced suppression of fear memory acquisition relies predominantly on the function of CB1Rs.

To further validate the importance of CB1Rs at $LPB^{Glu} \rightarrow CeL^{SOM}$ synapses in fear memory modulation, we selectively knocked down CB1R expression in the LPB using the siRNA. First, we verified the efficacy of the siRNA through RT-qPCR and western blot analysis. As shown in Figures 7H and 7I (For mRNA, $^{**}p = 0.0016$, two-sided unpaired *t*-test, Figure 7H; for protein, $^{**}p = 0.0013$, two-sided unpaired *t*-test; Figure 7I), the infusion of siRNA against CB1R significantly decreased the expression of CB1R mRNA in the LPB, and concurrently decreased CB1R protein levels in the CeL. Next, we conducted behavioral assessments as depicted in Figure 7J. We did not detect any differences in the freezing responses of the NC (negative control) +Vehicle and siRNA+Vehicle groups during FC or in the contextual fear memory test, indicating that intra-LPB infusion of siRNA targeting CB1R had no effect on conditioned fear memory learning or contextual fear memory retrieval (For the training period, $p = 0.79$, two-way ANOVA test, Figure 7K; For the contextual test, $^{***}p = 0.004$, one-way ANOVA test; Figure 7L). However, in the cued fear memory test, knocking down CB1R expression in the LPB contributed to a behavioral phenotype known as fear generalization, indicated by aggravated freezing responses in the siRNA+Vehicle group during the pre-Tone period. This could be rescued by activating the residual CB1Rs in the CeL with the cannabinoid agonist WIN55,212–2. During the tone period, freezing responses were not altered by CB1Rs knock down ($^{****}p < 0.0001$, two-way ANOVA test, Figure 7M). To test whether the effects of cannabinoids on fear memory acquisition were mediated through the $LPB^{Glu} \rightarrow CeL^{SOM}$ pathway, we combined siRNA knockdown with local pharmacological intervention. We found that selective CB1R knock down in the LPB tended to weaken the inhibitory effects of intra-CeL infusion of the cannabinoid agonist WIN55,212–2 on fear memory acquisition, as indicated by the increase in average freezing levels from 14.44% (NC + WIN55,212–2) to 40.67% (siRNA+WIN55,212–2) in the contextual fear memory test and from 27.12% (NC + WIN55,212–2) to 49.4% (siRNA+WIN55,212–2) during the tone period in the cued fear memory test, although these trends were not statistically significant. The lack of a strong effect may be due to a role for CB1Rs in other upstream nuclei in the intra-CeL WIN55,212–2 injection-induced impairment in fear memory acquisition (Figures 7L and 7M). Taken together, our results indicate that elevated excitability of the $LPB^{Glu} \rightarrow CeL^{SOM}$ pathway contributes to the acquisition of conditioned fear memories and that the FC-induced increase in CB1R expression plays a role in modulating this acquisition.

DISCUSSION

Increased activity of CeL^{SOM} neurons is critical for the acquisition of conditioned fear memories, and enhanced excitatory transmission onto CeL^{SOM} neurons has been demonstrated to be responsible for fear-conditioning-induced alterations in synaptic plasticity.[9,12] In this study, FC potentiated the excitatory inputs from LPB^{Glu} neurons to CeL^{SOM} neurons, and inhibiting this pathway resulted in impaired fear-memory acquisition. There is increasing interest in developing CB1R activators as antidepressant and anxiolytic drugs because of their important role in modulating synaptic plasticity. Here, we provide evidence that activation of CB1Rs in the $LPB^{Glu} \rightarrow CeL^{SOM}$ pathway inhibits the

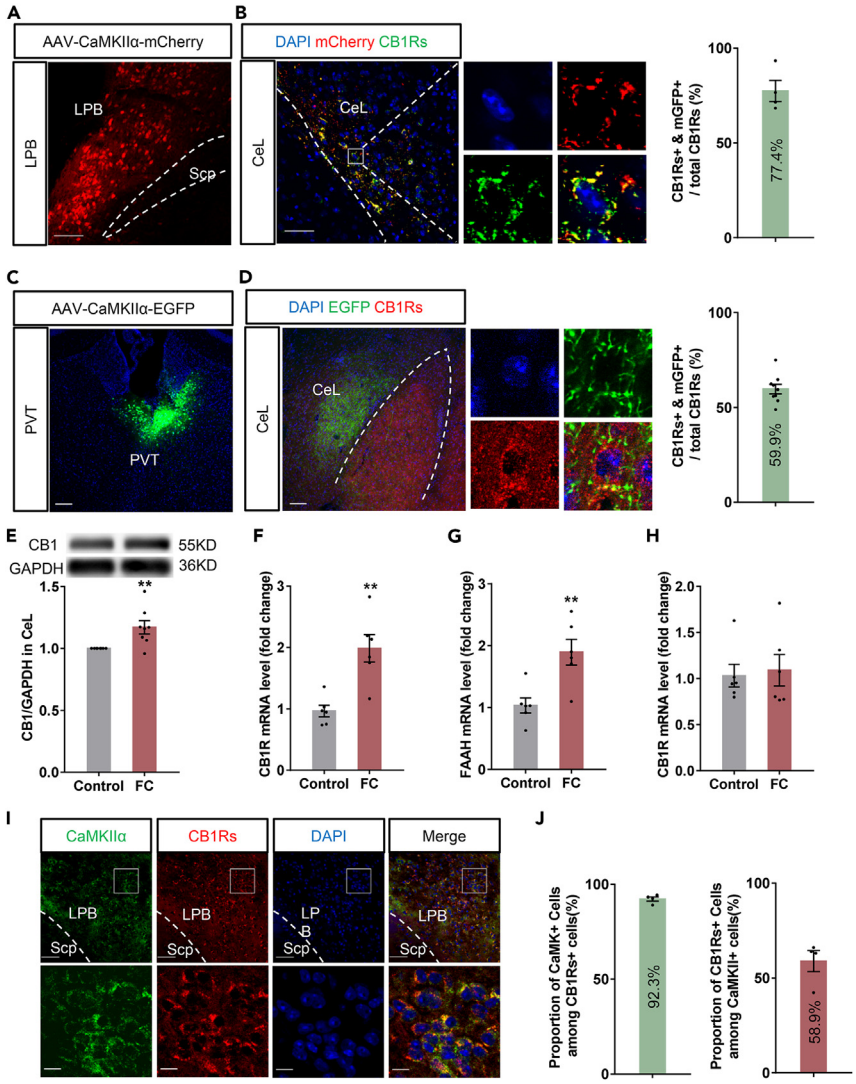

Figure 6. Increased synaptic activity in the LPB^{Glu}→CeL^{SOM} pathway in FC mice contributes to the upregulation of CB1Rs

(A) Representative images showing mCherry-labeled glutamatergic neurons in the LPB. Scale bar, 100 μm.

(B) Expression of CB1R (green) at the LPB→CeL glutamatergic terminals (red) and the proportion of total CB1R in the CeL expressed at LPB glutamatergic terminals. Scale bar, 50 μm.

(C) Representative images showing EGFP-labeled glutamatergic neurons in the PVT. Scale bar, 100 μm.

(D) Expression of CB1R (red) at the PVT→CeL glutamatergic terminals (green) and the proportion of total CB1R in the CeL expressed at PVT glutamatergic terminals. Scale bar, 100 μm.

(E and F) CB1R total protein in CeL (E, two-sided unpaired *t*-test, $t_{(1/14)} = 3.189$, $^{**}p = 0.0066$. $n = 8$ mice) and CB1R mRNA expression (F, two-sided unpaired *t*-test, $t_{(1/10)} = 4.194$, $^{**}p = 0.0018$, $n = 6$ mice) in LPB extracts were significantly increased in FC mice versus control mice.

(G) FC mice exhibited increased FAAH mRNA levels in the LPB compared with control mice (two-sided unpaired *t*-test, $t_{(1/10)} = 3.587$, $^{**}p = 0.005$. $n = 6$ mice).

(H) The level of CB1R mRNA in the PVT of FC mice did not differ from that of control mice (two-sided unpaired *t*-test, $t_{(1/10)} = 0.2893$, $p = 0.7783$, $n = 6$ mice).

(I) Top, Representative images of CaMKIIα mRNA and CB1R mRNA co-expression in the LPB of a wild-type mouse (Top, scale bar, 50 μm). Bottom, magnified images from the selected area in the top images (bottom, scale bar, 10 μm).

(J) Left, Percentage of CB1R mRNA-positive neurons that co-expressed CaMKIIα mRNA. Right, Percentage of CaMKIIα mRNA-positive neurons that co-expressed CB1R mRNA ($n = 4$ mice). All of the data are presented as mean ± SEM. $^{**}p < 0.01$.

acquisition of conditioned fear memories. In addition, we found that CeL^{SOM} neurons also receive excitatory input from the PVT, and that this pathway exerts an effect on the expression of fear memories after FC. These findings delineate critical neural pathways that dominate fear memory acquisition and expression.

People who experience traumatic events are likely to develop conditioned fear memories, which are difficult to extinguish in case the traumatic stressors surpass the allostatic capacity of the person. This can lead to hyper-anxiety conditions that manifest as continuous

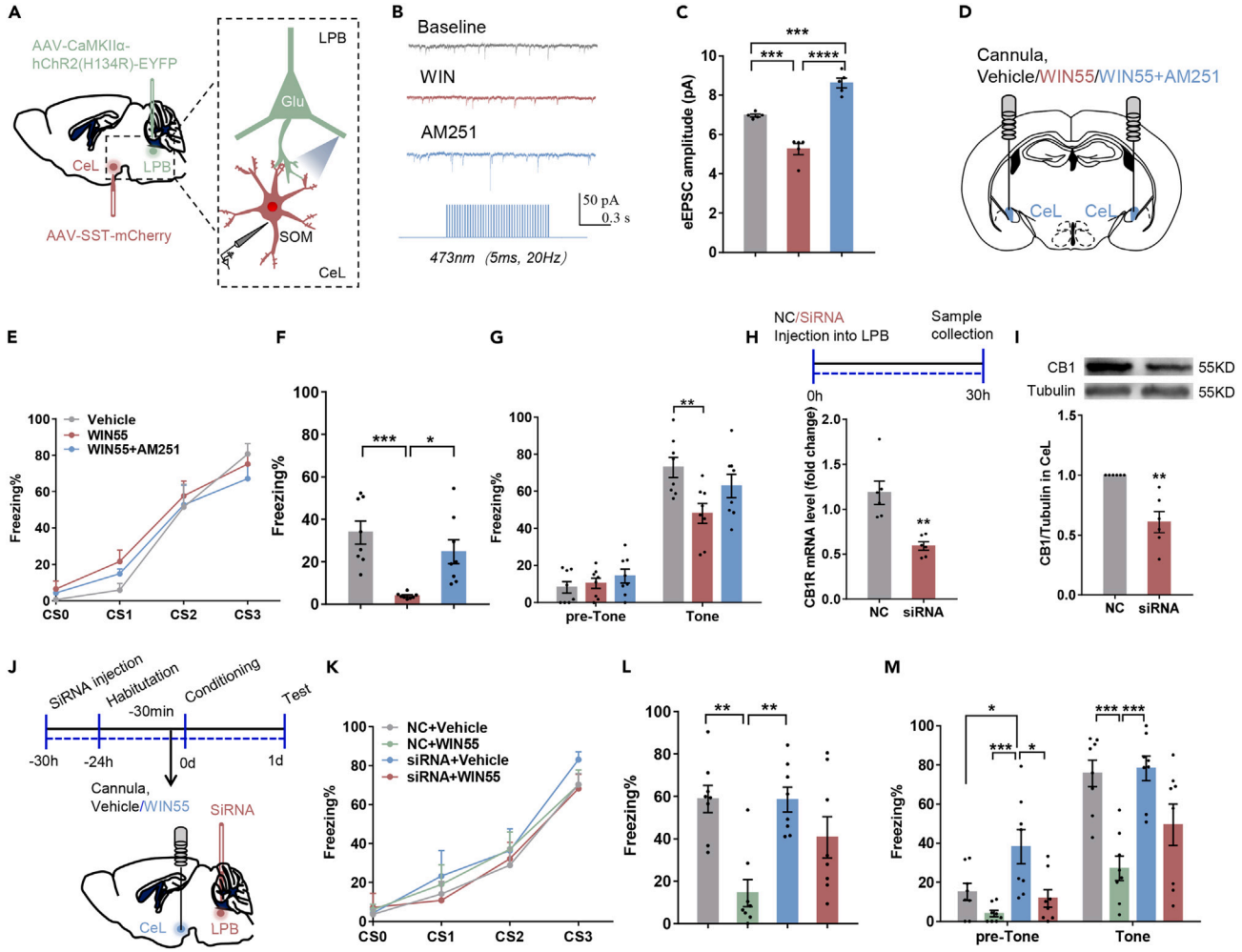

Figure 7. Modulation of CB1Rs in the LPB^{Glu}→CeL^{SOM} pathway affects conditioned fear memory acquisition

(A) Schematic of the *in vitro* slice recording paradigm.

(B) Representative average traces of eEPSCs in the absence (top) and presence of the CB1R agonist WIN55,212-2 (middle) or the CB1R antagonist AM251 (bottom).

(C) Bath application of WIN55,212-2 significantly decreased the amplitude of eEPSCs, whereas AM251 significantly increased the amplitude of eEPSCs compared with the baseline (one-way ANOVA, $F_{(2,12)} = 57.97$, ****$p < 0.0001$; Tukey's post hoc test, Baseline versus WIN55, ***$p = 0.0004$; Baseline versus AM251, ***$p = 0.0005$; WIN55 versus AM251, ****$p < 0.0001$; $n = 5$ neurons from 3 mice for each group).

(D) Schematic of the injection paradigm to test whether CB1Rs in the CeL control fear memory acquisition.

(E) Mice with CeL injections of the CB1R agonist WIN55 exhibited similar fear responses across the duration of fear conditioning as the other two groups (two-way ANOVA, group: $F_{(2,21)} = 0.5255$, $p = 0.5988$; time: $F_{(3,63)} = 93.78$, ****$p < 0.0001$; interaction: $F_{(6,63)} = 0.824$, $p = 0.5556$; $n = 8$ mice).

(F and G) Microinjection of the agonist WIN55 into the CeL significantly decreased freezing levels in the contextual (F, one-way ANOVA, $F_{(2,21)} = 11.52$, ***$p = 0.0004$; Tukey's post hoc test, Vehicle versus WIN55, ***$p = 0.0004$; WIN55 versus WIN55+AM251, *$p = 0.0101$; $n = 8$ mice) and cued (G, two-way ANOVA, group: $F_{(2,21)} = 2.892$, $p = 0.0777$; time: $F_{(1,21)} = 214.3$, ****$p < 0.0001$; interaction: $F_{(2,21)} = 5.214$, *$p = 0.0145$; Bonferroni's post hoc test, freezing for Vehicle versus WIN55 during Tone presentation, **$p = 0.0014$; $n = 8$ mice) fear memory tests, and the effect of WIN55 could be reversed with administration of the CB1R antagonist AM251.

(H and I) The expression levels of CB1R mRNA in the LPB (H, two-sided unpaired *t*-test, $t_{(1/10)} = 4.282$, **$p = 0.0016$, $n = 6$ mice) and CB1R protein in the CeL (I, two-sided unpaired *t*-test, $t_{(1/10)} = 4.426$, **$p = 0.0013$, $n = 6$ mice) both decreased significantly after LPB injection of siRNA targeting CB1Rs.

(J) Time course and schematic of the injection paradigm to identify the effects of CB1Rs at the LPB→CeL terminals on fear memory acquisition.

(K) There were no significant differences among the groups in freezing levels during the fear conditioning session (two-way ANOVA, group: $F_{(3,28)} = 0.3493$, $p = 0.79$; time: $F_{(3,84)} = 98.5$, ****$p < 0.0001$; interaction: $F_{(9,84)} = 0.4148$, $p = 0.9239$. $n = 8$ mice).

(L and M) Effects of selective CB1R knockdown in the LPB on CB1R agonist-induced contextual (L, one-way ANOVA, $F_{(3,28)} = 8.272$, ***$p = 0.0004$; Bonferroni's post hoc test, NC + Vehicle versus NC + WIN55, **$p = 0.0011$; NC + WIN55 versus siRNA+Vehicle, **$p = 0.0012$; $n = 8$ mice) and cued (M, two-way ANOVA,

Figure 7. *Continued*

$F_{(3,28)}$ = 12.8, ****p < 0.0001; Bonferroni's post hoc test, before Tone presentation: For NC + Vehicle versus siRNA+Vehicle, *p = 0.033; For NC + WIN55 versus siRNA+Vehicle, ***p = 0.0007; For siRNA +WIN55 versus siRNA+Vehicle, *p = 0.011; during Tone presentation: For NC + Vehicle versus NC + WIN55, ***p = 0.0007; For siRNA+Vehicle versus NC + WIN55, ***p = 0.0003; n = 8 mice) fear memory impairment. All of the data are presented as mean ± SEM. *p < 0.05, **p < 0.01, ***p < 0.001, ****p < 0.0001.

avoidance and increased alertness of the surrounding environment, eventually developing into fear-related disorders like PTSD (posttraumatic stress disorder).[43] In recent years, there has been a major shift in the conceptual framework for investigating neuropsychiatric disorders from the monoamine-oriented hypothesis to the neuroplasticity hypothesis, which points out that the structural and functional alterations in brain circuits mediate mental disorders and related treatments.[44] Clinical studies have revealed that subjects with PTSD showed reduced hippocampal volume and total white matter volume.[45,46] It has been reviewed that PTSD patients displayed decreased amplitude of low-frequency fluctuation (ALFF) in the amygdala and reduced gray matter volume (GMV) in the anterior cingulate cortex/medial prefrontal cortex (ACC/mPFC), striatum, insula, superior temporal gyrus, left postcentral gyrus, and occipital gyrus.[47] Pharmacological treatment with paroxetine or phenytoin could lead to a remission for symptoms of PTSD accompanied with an increase in hippocampal volume.[48] PTSD patients with symptoms remission exhibited cortical thinning and volume decrease in the left rostral ACC following prolonged exposure (PE) treatment, indicating an association between therapeutic effects and brain structural alterations.[49] Neuroimaging studies have demonstrated hyperactivation in emotion-generation regions, such as the amygdala or insula, and hypoactivation in emotion-regulation regions, including the mPFC and ACC. Patients with PTSD showed reduced positive connectivity between the mPFC and the amygdala, hippocampus, parahippocampal gyrus and rectus, as well as between the inferior orbitofrontal cortex and the hippocampus.[50,51] By using real-time fMRI neurofeedback (rt-fMRI-nf) in PTSD patients to downregulate both right and left amygdala activation, functional connectivity between the amygdala-PFC was increased during neurofeedback training.[52] These clinical studies indicate that abnormalities in brain structure, function, and functional connectivity in PTSD patients can be used as targets for clinical treatment and to evaluate therapeutic effects. Because of the limitations of clinical research, rodent stress models have been widely used to explore the pathogenesis of PTSD, and recent studies have confirmed that the FC model can successfully induce changes in synaptic plasticity in the amygdala of mice that contribute to fear-related behavioral phenotypes in mice.[6,22,53]

The CeL is composed of spiny GABAergic neurons that can be divided into multiple subtypes on the basis of their neuropeptide expression profiles, and different neuronal subtypes encoded distinct behavioral phenotypes throughout the FC procedure.[30,54] It has been found that intra-CeL injections of GABA receptor agonists can inhibit fear memory acquisition, indicating that CeL plays an important role in the formation of conditioned fear memory.[55] In our study, we utilized lidocaine to reversibly inhibit the excitability of CeL and found that it could inhibit contextual fear memory acquisition, with a lack of effects on cued fear memory acquisition. Whereas specific ablation of GABAergic neurons in the CeL could impair both contextual and cued fear memory acquisition. The discrepancy in results may be attributed to the differences in targeted neurons of lidocaine and the pro-apoptotic virus. Therefore, we need to further specifically modulate GABAergic neurons in CeL to clarify its role in conditioned fear memory acquisition. SOM^+ GABA neurons, which exhibit increased activity in response to CS, are considered to be fear-on neurons, playing an essential role in evoking freezing behaviors. In contrast PKC-δ^+ GABA neurons, known as fear-off neurons, show reduced reactivity during CS exposure, and inhibition of PKC-δ^+ GABA neurons has been confirmed to be able to enhance fear responses.[9,10,27] In addition, CRF^+ GABA neurons are thought to promote flight responses during FC.[54,56] Furthermore, SOM^+ GABA neurons has been reported to form connections with other neuron subtypes in the CeL, engaging in the modulation of intra-CeL microcircuits, thereby participating in associative downstream threat processing.[1,9,12,57] This supports our findings that optogenetic inhibition of CeL^{SOM} neurons impaired contextual and cued fear memory acquisition. This was further corroborated by electrophysiological data showing that CeL^{SOM} neurons had increased excitability following FC as well as an increased frequency and amplitude of mEPSCs, indicating that enhanced excitatory synaptic transmission onto CeL^{SOM} neurons may account for the fear-conditioning-induced enhanced synaptic plasticity in the CeL. The anatomical connectivity of the CeL has been studied in detail: the CeL receives afferents from a variety of emotion-associated extra-amygdalar sites, including the auditory cortex, the auditory thalamus, LPB, and PVT,[8] among which the LPB and PVT were proven to participate in FC in our study. We did not incorporate auditory cortex and the auditory thalamus in our study because the role of these two areas in fear memory acquisition has been well established, whereas the roles of the LPB and PVT required further exploration.[58–61]

According to previous reports, the LPB is the predominant target of ascending nociceptive neurons from the dorsal horn, and this nociceptive information is subsequently transmitted to the CeA by projection neurons that directly target the CeA.[62,63] These connections ultimately form the spino-parabrachial-amygdaloid pathway, which is actively involved in processing noxious information and may therefore play a critical role in fear learning that involves a noxious US.[14,63,64] Neuron tracing results provided anatomical evidence for the synapses formed between the PBN-derived glutamate terminals and GABAergic neurons in the CeL.[65,66] And it has been proven that FC results in synaptic potentiation in the LPB-CeA synapse, and this potentiation relates to associative learning of fear memory, not primarily depends on fear retrieval or nociceptive experience.[67] Moreover, recent studies have found that the calcium activity of $CGRP^+$ neurons in the LPB is closely related to contextual and cued fear memory formation. Silencing LPB $CGRP^+$ neurons and CeL $Calcrl^+$ neurons that receive projections from LPB $CGRP^+$ neurons both inhibit the formation of conditioned fear memory.[64] CeL can be further divided into rostal CeA (rCeA) and caudal CeA (cCeA) according to their spatial location across the rostro-caudal axis. $Calcrl^+$ neurons in rCeA preferentially receive external somatosensory stimuli and project to brain areas implicated in arousal and motivation, while cCeA $Calcrl^+$ neurons receive internal sensory stimuli and project to downstream regions implicated in malaise. $Calcrl^+$ neurons in rCeA and cCeA are reported to play distinct roles in fear

memory learning, with rCeA Calcrl^{+} neurons primarily encoding US occurrence, while cCeA Calcrl^{+} neurons initially respond to US and maintain CS responses after fear memory consolidation.[68]

Studies have shown that CeL PKC-δ^{+} neurons substantially overlapped with Calcrl^{+} neurons in the cCeA, and optogenetic inhibiting PKC-δ^{+} neurons during US exposure can successfully disrupt the formation of fear memory, supporting a critical role of CeL PKC-δ^{+} neurons in relaying US signal from the LPB during FC.[11,55] In combination with previous studies, PKC neurons are fear-off neurons, but it cannot be excluded that some of the CeL PKC-δ^{+} neurons may indeed be fear-on neurons, as PKC-δ^{+} neurons are heterogeneous, and their different responses to conditioned fear may be related to their distinct molecular clusters.[10,55,69] SOM^{+} neurons in the CeL, acted as fear-on neurons, are partially co-labeled with CeL Calcrl^{+} neurons as well. It has been reported that SOM^{+} neurons in CeL can actually convey CS information during FC, and the specific role of their functional connectivity with LPB in FC deserves further investigation.[9,27] Using chemogenetic and optogenetic techniques, we identified that inhibition of the CeL-projecting LPB glutamatergic neurons could substantially impair contextual and cued fear memory acquisition in mice subjected to FC. Clinical studies have found that PTSD patients exhibited impaired WM updating function, which can affect the forgetting of trauma-related memories.[70] However, in our study, inhibition of the LPB^{Glu}→CeL^{SOM} pathway during Y-maze test did not exert an effect in spatial WM. In addition, we used a monosynaptic anterograde virus for specific optogenetic inhibition of CeL^{SOM} neurons that are innervated by the LPB, with impaired conditioned fear memory acquisition observed as a result. These findings indicate that inhibition of the LPB^{Glu}→CeL^{SOM} pathway suppressed the activity of these nociceptive CeL neurons and consequently weakened US-dependent fear memories, emphasizing the role of the LPB^{Glu}→CeL^{SOM} pathway in fear memory acquisition.

As confirmed in previous studies, the excitation of nociceptive neurons in the spinal dorsal horn by foot shock can substantially activate both spino-parabrachial and spino-thalamic pathways.[11,63] A previous published review has revealed that the activation of effective connectivity between the thalamus and the amygdala, striatum, rostral ACC, and ventral occipital cortex increased in PTSD patients, and in-task amygdala-thalamus connectivity is correlated with PTSD severity.[71] PTSD patients exhibited significant GMV reduction in the left thalamus and its subregions, and the GMV values of the thalamic subregions were positively correlated with the PTSD symptoms score.[72] The PVT serves as an important nucleus in the thalamus for gating associative learning by providing a dynamic representation of stimulus salience.[73–75] Anatomical studies have shown that the PVT projects strongly to the CeL.[76,77] In our study, chemogenetic inhibition of the CeL-projecting PVT glutamatergic neurons impaired cued fear memory acquisition, which was in contrast with the observation that immediate optogenetic inhibition of PVT-glutamatergic terminals in the CeL during FC did not exert effects on fear memory acquisition. The discrepancy between these two manipulations may be due to differences in the temporal dynamics. The duration of optogenetic inhibition of the PVT^{Glu}→CeL^{SOM} pathway was limited to the period of fear memory acquisition, whereas chemogenetic inhibition has a lasting effect that could be expected to interfere with consolidation-related processes following fear memory acquisition.[38] This explanation is consistent with previous findings that selective inactivation of CeL-projecting PVT neurons impairs conditioning-induced synaptic potentiation onto CeL^{SOM} neurons 24 h after FC but does not have an effect on CeL plasticity 3 h after conditioning.[12] These results suggest that the PVT^{Glu}→CeL^{SOM} pathway does not underlie conditioned fear memory acquisition and that the role of this pathway in fear memory consolidation requires further investigation by, for example, selectively manipulating the circuit for an extended period of time starting immediately after FC.

The recruitment of the LPB^{Glu}→CeL^{SOM} pathway during fear memory acquisition raises the question of the possible mechanisms involved. Previous studies have shown that CB1Rs are extensively distributed in the central nervous system and functionally inhibit the release of presynaptic neurotransmitters through retrograde signaling.[15] Clinical evidence has been provided that reduced hair concentrations of endocannabinoids in PTSD patients was negatively correlated with symptom severity of PTSD, and the availability of the CB1Rs in PTSD patients was abnormally altered as well.[78,79] Although CB1Rs have been reported to be located at excitatory terminals in the CeL,[21] little is known about the expression of CB1Rs in the LPB^{Glu}→CeL^{SOM} pathway. Using *in situ* hybridization, immunohistochemical staining, in combination with rabies virus, we demonstrated that CB1Rs expressed in the presynapses targeting CeL^{SOM} neurons partly came from LPB glutamatergic projections. CB1Rs in the LPB^{Glu}→CeL^{SOM} pathway played an important role in regulating synaptic plasticity by suppressing the LPB glutamatergic transmission to the CeL.

CB1R-knockout mice display enhanced expression of conditioned fear memories when confronted with aversive conditions, accompanied by impaired extinction of fear memories.[80] Mice subjected to FC exhibit increased expression of CB1Rs and decreased expression of endocannabinoids in the amygdala.[81–83] Our results support these previous findings by showing that expression of CB1Rs and of the endogenous cannabinoid hydrolase FAAH are elevated in the LPB^{Glu}→CeL^{SOM} pathway in FC mice. The upregulation of CB1Rs in the parabrachial-amygdaloid pathway may act to compensate for decreased anandamide (AEA) levels, which are related to the protective responses of the brain. Several lines of evidence have shown that hyperactivity of CRF receptor type 1 (CRFr1) after stress exposure contributes to depletion of AEA in the CeA, which correlates with increases in FAAH activity.[84,85] As a result, the deficiency in AEA signaling ultimately primes stress-reactive systems in the CeA to facilitate stress-related behaviors. In addition, it has been reported that increased CB1R signaling can reduce HPA(Hypothalamic-pituitary-adrenocortical) axis activation, thereby attenuating the negative effects of traumatic stress.[86,87]

In recent years, there have been increasingly case reports on the application of cannabinoid receptor modulators in patients with PTSD, indicating that cannabinoid receptor modulators are an effective treatment for PTSD.[88] A recent retrospective study that first explored the benefits of cannabidiol (CBD) in patients with PTSD showed that oral administration of CBD significantly improved the scores on the PTSD symptom checklist (PCL-5) without evident adverse effects.[89] A preliminary, open-label study found that patients suffered with chronic PTSD can ameliorate their high arousal symptoms, reduce the frequency of nightmares, and improve global symptom severity by using delta-tetrahydrocannabinol (Δ^{9}-THC) as an adjuvant therapy on the basis of stable drug treatment.[90] In addition, studies have shown that nabilone (a synthetic cannabinoid) treatment was associated with a significant reduction in nightmares (severity and frequency) and PTSD symptom

severity as well as an improvement in general well-being.[91–93] These studies all support the potential benefits of cannabinoid receptor agonists in improving PTSD symptom clusters. However, clinical evidence has shown that excessive use of cannabinoids can lead to psychiatric symptoms and a decline in memory compared with low-dose use.[94–96] Such reports further emphasize the importance of safety testing and dose control prior to the initiation of synthetic cannabinoid agonist therapy in patients with PTSD. In this study, we interfered with the function of CB1Rs locally at the $LPB^{Glu} \rightarrow CeL^{SOM}$ pathway to avoid the side effects of systemic cannabinoid administration. Selectively knocking down CB1R mRNA expression in the LPB had a tendency to mitigate the inhibitory effects exerted by presynaptic pharmacological activation of CB1Rs in the CeL on the acquisition of fear memories, although the result was not statistically significant. These results revealed that presynaptic CB1Rs located on terminals in the CeL regulate fear memory acquisition, but that the fear memory impairment induced by CeL injection of WIN55,212–2 is not completely mediated by the $LPB^{Glu} \rightarrow CeL^{SOM}$ pathway. In addition to the LPB, the BLA has dense expression of CB1Rs, with activation of CB1Rs in the BLA contributing to decreased signaling to the CeA via an interaction with the cholecystokinin (CCK) system, thus promoting extinction of fear memories.[97] Therefore, CB1Rs at the BLA→CeL terminals may also participate in cannabinoid-induced impairments in fear memory, whereas the specific anatomical connections and functions await further investigation.

Overall, we demonstrated that FC induces prolonged increases in the activity of CeL^{SOM} neurons and that this can be modulated by projection neurons from the LPB and PVT. Excitation of the $LPB^{Glu} \rightarrow CeL^{SOM}$ pathway dominates fear memory acquisition and the $PVT^{Glu} \rightarrow CeL^{SOM}$ pathway may be involved in consolidation-related processes following fear memory acquisition. In addition, our results provide sufficient evidence that activation of CB1Rs at the presynaptic terminals in the CeL impairs the acquisition of fear memories, in part through the $LPB^{Glu} \rightarrow CeL^{SOM}$ pathway. Therefore, our study unveils the potential neurobiological mechanisms underlying FC, providing theoretical supports for future exploration into the pathophysiology of fear-related disorders.

Limitations of the study

In this study, we manipulated the $PVT^{Glu} \rightarrow CeL^{SOM}$ pathway during the period of FC, and did not selectively inhibit CeL-projecting PVT neurons for an extended period of time starting immediately after conditioning. *In vivo* electrophysiology combined with optogenetics could be used to explore the neuronal populations in PVT activated after FC at the early versus late time points in the future.

We adopted FC as an animal model to study the neurobiological mechanisms underlying the formation of fear memory. However, FC should not be regarded as a model exclusively for PTSD research, as it fails to accurately mimic the behavioral phenotypes associated with PTSD. Future studies should utilize the 129S1/SvImJ mouse strain or the sensitization-based model to combine with FC to study the pathogenesis of PTSD.

RESOURCE AVAILABILITY

Lead contact

Further information and requests for resources and reagents should be directed to and will be fulfilled by the lead contact, Yong-mei Zhang (zhangym700@163.com).

Materials availability

This study did not generate new unique reagents.

Data and code availability

- Data reported in this paper will be shared by the lead contact upon request.
- This paper does not report original code.
- Any additional information required to reanalyze the data reported in this paper is available from the lead contact upon request.

ACKNOWLEDGMENTS

This study was supported by STI2030-Major Projects (2021ZD0203100), grants from the National Natural Science Foundation of China (no.81772065; no.82271257; no.82071228), Qing Lan Project, and Open Competition grant from Xuzhou Medical University (JBGS202202). We are deeply indebted to Shuai Shao for his dedication to behavioral experiments.

AUTHOR CONTRIBUTIONS

Conceptualization, Y.M.Z. and J.H.G.; methodology, J.H.G., Y.Y.L., H.X.X., K.W., and L.L.Z.; investigation, J.H.G., P.C., and X.H.P.; writing—original draft, J.H.G. and Y.M.Z.; writing—review and editing, Y.M.Z., J.H.G., and Y.Y.L.; funding acquisition, Y.M.Z.; supervision, R.H. and J.L.C.

DECLARATION OF INTERESTS

The authors declare no competing interests.

STAR★METHODS

Detailed methods are provided in the online version of this paper and include the following:

- KEY RESOURCES TABLE
- EXPERIMENTAL MODEL AND STUDY PARTICIPANT DETAILS

SUPPLEMENTAL INFORMATION

Supplemental information can be found online at https://doi.org/10.1016/j.isci.2024.110886.

Received: January 15, 2024
Revised: April 18, 2024
Accepted: September 3, 2024
Published: September 4, 2024

REFERENCES

1. Ross, D.A., Arbuckle, M.R., Travis, M.J., Dwyer, J.B., Van Schalkwyk, G.I., and Ressler, K.J. (2017). An Integrated Neuroscience Perspective on Formulation and Treatment Planning for Posttraumatic Stress Disorder: An Educational Review. JAMA Psychiatr. *74*, 407–415. https://doi.org/10.1001/jamapsychiatry.2016.3325.
2. Michopoulos, V., Vester, A., and Neigh, G. (2016). Posttraumatic stress disorder: A metabolic disorder in disguise? Exp. Neurol. *284*, 220–229. https://doi.org/10.1016/j.expneurol.2016.05.038.
3. Ressler, K.J., Berretta, S., Bolshakov, V.Y., Rosso, I.M., Meloni, E.G., Rauch, S.L., and Carlezon, W.A., Jr. (2022). Post-traumatic stress disorder: clinical and translational neuroscience from cells to circuits. Nat. Rev. Neurol. *18*, 273–288. https://doi.org/10.1038/s41582-022-00635-8.
4. Yoo, S., Stremlau, M., Pinto, A., Woo, H., Curtis, O., and van Praag, H. (2021). Effects of Combined Anti-Hypertensive and Statin Treatment on Memory, Fear Extinction, Adult Neurogenesis, and Angiogenesis in Adult and Middle-Aged Mice. Cells *10*, 1778. https://doi.org/10.3390/cells10071778.
5. Coventry, P.A., Meader, N., Melton, H., Temple, M., Dale, H., Wright, K., Cloitre, M., Karatzias, T., Bisson, J., Roberts, N.P., et al. (2020). Psychological and pharmacological interventions for posttraumatic stress disorder and comorbid mental health problems following complex traumatic events: Systematic review and component network meta-analysis. PLoS Med. *17*, e1003262. https://doi.org/10.1371/journal.pmed.1003262.
6. Johansen, J.P., Cain, C.K., Ostroff, L.E., and LeDoux, J.E. (2011). Molecular mechanisms of fear learning and memory. Cell *147*, 509–524. https://doi.org/10.1016/j.cell.2011.10.009.
7. Sah, P., Faber, E.S.L., Lopez De Armentia, M., and Power, J. (2003). The amygdaloid complex: anatomy and physiology. Physiol. Rev. *83*, 803–834. https://doi.org/10.1152/physrev.00002.2003.
8. Keifer, O.P., Jr., Hurt, R.C., Ressler, K.J., and Marvar, P.J. (2015). The Physiology of Fear: Reconceptualizing the Role of the Central Amygdala in Fear Learning. Physiology *30*, 389–401. https://doi.org/10.1152/physiol.00058.2014.
9. Li, H., Penzo, M.A., Taniguchi, H., Kopec, C.D., Huang, Z.J., and Li, B. (2013). Experience-dependent modification of a central amygdala fear circuit. Nat. Neurosci. *16*, 332–339. https://doi.org/10.1038/nn.3322.
10. Haubensak, W., Kunwar, P.S., Cai, H., Ciocchi, S., Wall, N.R., Ponnusamy, R., Biag, J., Dong, H.W., Deisseroth, K., Callaway, E.M., et al. (2010). Genetic dissection of an amygdala microcircuit that gates conditioned fear. Nature *468*, 270–276. https://doi.org/10.1038/nature09553.
11. Han, S., Soleiman, M.T., Soden, M.E., Zweifel, L.S., and Palmiter, R.D. (2015). Elucidating an Affective Pain Circuit that Creates a Threat Memory. Cell *162*, 363–374. https://doi.org/10.1016/j.cell.2015.05.057.
12. Penzo, M.A., Robert, V., Tucciarone, J., De Bundel, D., Wang, M., Van Aelst, L., Darvas, M., Parada, L.F., Palmiter, R.D., He, M., et al. (2015). The paraventricular thalamus controls a central amygdala fear circuit. Nature *519*, 455–459. https://doi.org/10.1038/nature13978.
13. Do-Monte, F.H., Quiñones-Laracuente, K., and Quirk, G.J. (2015). A temporal shift in the circuits mediating retrieval of fear memory. Nature *519*, 460–463. https://doi.org/10.1038/nature14030.
14. Palmiter, R.D. (2018). The Parabrachial Nucleus: CGRP Neurons Function as a General Alarm. Trends Neurosci. *41*, 280–293. https://doi.org/10.1016/j.tins.2018.03.007.
15. Kreitzer, F.R., and Stella, N. (2009). The therapeutic potential of novel cannabinoid receptors. Pharmacol. Ther. *122*, 83–96. https://doi.org/10.1016/j.pharmthera.2009.01.005.
16. Ye, L., Cao, Z., Wang, W., and Zhou, N. (2019). New Insights in Cannabinoid Receptor Structure and Signaling. Curr. Mol. Pharmacol. *12*, 239–248. https://doi.org/10.2174/1874467212666190215112036.
17. Piomelli, D. (2003). The molecular logic of endocannabinoid signalling. Nat. Rev. Neurosci. *4*, 873–884. https://doi.org/10.1038/nrn1247.
18. Jacob, W., Marsch, R., Marsicano, G., Lutz, B., and Wotjak, C.T. (2012). Cannabinoid CB1 receptor deficiency increases contextual fear memory under highly aversive conditions and long-term potentiation *in vivo*. Neurobiol. Learn. Mem. *98*, 47–55. https://doi.org/10.1016/j.nlm.2012.04.008.
19. Cannich, A., Wotjak, C.T., Kamprath, K., Hermann, H., Lutz, B., and Marsicano, G. (2004). CB1 cannabinoid receptors modulate kinase and phosphatase activity during extinction of conditioned fear in mice. Learn. Mem. *11*, 625–632. https://doi.org/10.1101/lm.77904.
20. Kamprath, K., Romo-Parra, H., Häring, M., Gaburro, S., Doengi, M., Lutz, B., and Pape, H.C. (2011). Short-term adaptation of conditioned fear responses through endocannabinoid signaling in the central amygdala. Neuropsychopharmacology *36*, 652–663. https://doi.org/10.1038/npp.2010.196.
21. Ramikie, T.S., Nyilas, R., Bluett, R.J., Gamble-George, J.C., Hartley, N.D., Mackie, K., Watanabe, M., Katona, I., and Patel, S. (2014). Multiple mechanistically distinct modes of endocannabinoid mobilization at central amygdala glutamatergic synapses. Neuron *81*, 1111–1125. https://doi.org/10.1016/j.neuron.2014.01.012.
22. Zhang, G., Ásgeirsdóttir, H.N., Cohen, S.J., Munchow, A.H., Barrera, M.P., and Stackman, R.W., Jr. (2013). Stimulation of serotonin 2A receptors facilitates consolidation and extinction of fear memory

in C57BL/6J mice. Neuropharmacology *64*, 403–413. https://doi.org/10.1016/j.neuropharm.2012.06.007.

23. Kwon, O.B., Lee, J.H., Kim, H.J., Lee, S., Lee, S., Jeong, M.J., Kim, S.J., Jo, H.J., Ko, B., Chang, S., et al. (2015). Dopamine Regulation of Amygdala Inhibitory Circuits for Expression of Learned Fear. Neuron *88*, 378–389. https://doi.org/10.1016/j.neuron.2015.09.001.
24. Daws, S.E., Joseph, N.F., Jamieson, S., King, M.L., Chévere-Torres, I., Fuentes, I., Shumyatsky, G.P., Brantley, A.F., Rumbaugh, G., and Miller, C.A. (2017). Susceptibility and Resilience to Posttraumatic Stress Disorder-like Behaviors in Inbred Mice. Biol. Psychiatr. *82*, 924–933. https://doi.org/10.1016/j.biopsych.2017.06.030.
25. Yu, H., Watt, H., Kesavan, C., Johnson, P.J., Wergedal, J.E., and Mohan, S. (2012). Lasting consequences of traumatic events on behavioral and skeletal parameters in a mouse model for post-traumatic stress disorder (PTSD). PLoS One *7*, e42684. https://doi.org/10.1371/journal.pone.0042684.
26. Wilensky, A.E., Schafe, G.E., Kristensen, M.P., and LeDoux, J.E. (2006). Rethinking the fear circuit: the central nucleus of the amygdala is required for the acquisition, consolidation, and expression of Pavlovian fear conditioning. J. Neurosci. *26*, 12387–12396. https://doi.org/10.1523/JNEUROSCI.4316-06.2006.
27. Ciocchi, S., Herry, C., Grenier, F., Wolff, S.B.E., Letzkus, J.J., Vlachos, I., Ehrlich, I., Sprengel, R., Deisseroth, K., Stadler, M.B., et al. (2010). Encoding of conditioned fear in central amygdala inhibitory circuits. Nature *468*, 277–282. https://doi.org/10.1038/nature09559.
28. Van Den Burg, E.H., and Stoop, R. (2019). Neuropeptide signalling in the central nucleus of the amygdala. Cell Tissue Res. *375*, 93–101. https://doi.org/10.1007/s00441-018-2862-6.
29. Sosulina, L., Strippel, C., Romo-Parra, H., Walter, A.L., Kanyshkova, T., Sartori, S.B., Lange, M.D., Singewald, N., and Pape, H.C. (2015). Substance P excites GABAergic neurons in the mouse central amygdala through neurokinin 1 receptor activation. J. Neurophysiol. *114*, 2500–2508. https://doi.org/10.1152/jn.00883.2014.
30. Kim, J., Zhang, X., Muralidhar, S., Leblanc, S.A., and Tonegawa, S. (2017). Basolateral to Central Amygdala Neural Circuits for Appetitive Behaviors. Neuron *93*, 1464–1479.e5. https://doi.org/10.1016/j.neuron.2017.02.034.
31. Delaney, A.J., Crane, J.W., Holmes, N.M., Fam, J., and Westbrook, R.F. (2018). Baclofen acts in the central amygdala to reduce synaptic transmission and impair context fear conditioning. Sci. Rep. *8*, 9908. https://doi.org/10.1038/s41598-018-28321-0.
32. Bao, J., Jin, Y., Jiang, Y., Khanna, R., and Yu, J. (2020). The Septum-Hippocampal Cholinergic Circuit: A Novel Pathway for Seizure Control. Biol. Psychiatr. *87*, 785–786. https://doi.org/10.1016/j.biopsych.2020.02.003.
33. Benfenati, F., Valtorta, F., Rubenstein, J.L., Gorelick, F.S., Greengard, P., and Czernik, A.J. (1992). Synaptic vesicle-associated Ca2+/calmodulin-dependent protein kinase II is a binding protein for synapsin I. Nature *359*, 417–420. https://doi.org/10.1038/359417a0.
34. Opazo, P., Labrecque, S., Tigaret, C.M., Frouin, A., Wiseman, P.W., De Koninck, P., and Choquet, D. (2010). CaMKII triggers the diffusional trapping of surface AMPARs through phosphorylation of stargazin. Neuron *67*, 239–252. https://doi.org/10.1016/j.neuron.2010.06.007.
35. Herring, B.E., and Nicoll, R.A. (2016). Long-Term Potentiation: From CaMKII to AMPA Receptor Trafficking. Annu. Rev. Physiol. *78*, 351–365. https://doi.org/10.1146/annurev-physiol-021014-071753.
36. Zuj, D.V., Palmer, M.A., Lommen, M.J.J., and Felmingham, K.L. (2016). The centrality of fear extinction in linking risk factors to PTSD: A narrative review. Neurosci. Biobehav. Rev. *69*, 15–35. https://doi.org/10.1016/j.neubiorev.2016.07.014.
37. Brewin, C.R., and Smart, L. (2005). Working memory capacity and suppression of intrusive thoughts. J. Behav. Ther. Exp. Psychiatr. *36*, 61–68. https://doi.org/10.1016/j.jbtep.2004.11.006.
38. Do Monte, F.H., Quirk, G.J., Li, B., and Penzo, M.A. (2016). Retrieving fear memories, as time goes by. Mol. Psychiatr. *21*, 1027–1036. https://doi.org/10.1038/mp.2016.78.
39. Kirouac, G.J. (2021). The Paraventricular Nucleus of the Thalamus as an Integrating and Relay Node in the Brain Anxiety Network. Front. Behav. Neurosci. *15*, 627633. https://doi.org/10.3389/fnbeh.2021.627633.
40. Chang, Y.T., Chen, W.H., Shih, H.C., Min, M.Y., Shyu, B.C., and Chen, C.C. (2019). Anterior nucleus of paraventricular thalamus mediates chronic mechanical hyperalgesia. Pain *160*, 1208–1223. https://doi.org/10.1097/j.pain.0000000000001497.
41. Shen, C.J., Zheng, D., Li, K.X., Yang, J.M., Pan, H.Q., Yu, X.D., Fu, J.Y., Zhu, Y., Sun, Q.X., Tang, M.Y., et al. (2019). Cannabinoid CB1 receptors in the amygdalar cholecystokinin glutamatergic afferents to nucleus accumbens modulate depressive-like behavior. Nat. Med. *25*, 337–349. https://doi.org/10.1038/s41591-018-0299-9.
42. Wang, H., Dong, P., He, C., Feng, X.Y., Huang, Y., Yang, W.W., Gao, H.J., Shen, X.F., Lin, S., Cao, S.X., et al. (2020). Incerta-thalamic Circuit Controls Nocifensive Behavior via Cannabinoid Type 1 Receptors. Neuron *107*, 538–551.e7. https://doi.org/10.1016/j.neuron.2020.04.027.
43. Bian, X.L., Qin, C., Cai, C.Y., Zhou, Y., Tao, Y., Lin, Y.H., Wu, H.Y., Chang, L., Luo, C.X., and Zhu, D.Y. (2019). Anterior Cingulate Cortex to Ventral Hippocampus Circuit Mediates Contextual Fear Generalization. J. Neurosci. *39*, 5728–5739. https://doi.org/10.1523/JNEUROSCI.2739-18.2019.
44. Musazzi, L., Tornese, P., Sala, N., and Popoli, M. (2018). What Acute Stress Protocols Can Tell Us About PTSD and Stress-Related Neuropsychiatric Disorders. Front. Pharmacol. *9*, 758. https://doi.org/10.3389/fphar.2018.00758.
45. Villarreal, G., Hamilton, D.A., Petropoulos, H., Driscoll, I., Rowland, L.M., Griego, J.A., Kodituwakku, P.W., Hart, B.L., Escalona, R., and Brooks, W.M. (2002). Reduced hippocampal volume and total white matter volume in posttraumatic stress disorder. Biol. Psychiatr. *52*, 119–125. https://doi.org/10.1016/s0006-3223(02)01359-8.
46. Basavaraju, R., France, J., Maas, B., Brickman, A.M., Flory, J.D., Szeszko, P.R., Yehuda, R., Neria, Y., Rutherford, B.R., and Provenzano, F.A. (2021). Right parahippocampal volume deficit in an older population with posttraumatic stress disorder. J. Psychiatr. Res. *137*, 368–375. https://doi.org/10.1016/j.jpsychires.2021.03.015.
47. Xiao, S., Yang, Z., Su, T., Gong, J., Huang, L., and Wang, Y. (2022). Functional and structural brain abnormalities in posttraumatic stress disorder: A multimodal meta-analysis of neuroimaging studies. J. Psychiatr. Res. *155*, 153–162. https://doi.org/10.1016/j.jpsychires.2022.08.010.
48. Bremner, J.D. (2006). The relationship between cognitive and brain changes in posttraumatic stress disorder. Ann. N. Y. Acad. Sci. *1071*, 80–86. https://doi.org/10.1196/annals.1364.008.
49. Helpman, L., Papini, S., Chhetry, B.T., Shvil, E., Rubin, M., Sullivan, G.M., Markowitz, J.C., Mann, J.J., and Neria, Y. (2016). PTSD Remission after Prolonged Exposure Treatment Is Associated with Anterior Cingulate Cortex Thinning and Volume Reduction. Depress. Anxiety *33*, 384–391. https://doi.org/10.1002/da.22471.
50. Jin, C., Qi, R., Yin, Y., Hu, X., Duan, L., Xu, Q., Zhang, Z., Zhong, Y., Feng, B., Xiang, H., et al. (2014). Abnormalities in whole-brain functional connectivity observed in treatment-naive post-traumatic stress disorder patients following an earthquake. Psychol. Med. *44*, 1927–1936. https://doi.org/10.1017/S003329171300250X.
51. Sripada, R.K., King, A.P., Garfinkel, S.N., Wang, X., Sripada, C.S., Welsh, R.C., and Liberzon, I. (2012). Altered resting-state amygdala functional connectivity in men with posttraumatic stress disorder. J. Psychiatry Neurosci. *37*, 241–249. https://doi.org/10.1503/jpn.110069.
52. Nicholson, A.A., Rabellino, D., Densmore, M., Frewen, P.A., Paret, C., Kluetsch, R., Schmahl, C., Théberge, J., Neufeld, R.W.J., McKinnon, M.C., et al. (2017). The neurobiology of emotion regulation in posttraumatic stress disorder: Amygdala downregulation via real-time fMRI neurofeedback. Hum. Brain Mapp. *38*, 541–560. https://doi.org/10.1002/hbm.23402.
53. Bauer, E.P. (2015). Serotonin in fear conditioning processes. Behav. Brain Res. *277*, 68–77. https://doi.org/10.1016/j.bbr.2014.07.028.
54. Kovner, R., Fox, A.S., French, D.A., Roseboom, P.H., Oler, J.A., Fudge, J.L., and Kalin, N.H. (2019). Somatostatin Gene and Protein Expression in the Non-human Primate Central Extended Amygdala. Neuroscience *400*, 157–168. https://doi.org/10.1016/j.neuroscience.2018.12.035.
55. Yu, K., Ahrens, S., Zhang, X., Schiff, H., Ramakrishnan, C., Fenno, L., Deisseroth, K., Zhao, F., Luo, M.H., Gong, L., et al. (2017). The central amygdala controls learning in the lateral amygdala. Nat. Neurosci. *20*, 1680–1685. https://doi.org/10.1038/s41593-017-0009-9.
56. Fadok, J.P., Krabbe, S., Markovic, M., Courtin, J., Xu, C., Massi, L., Botta, P., Bylund, K., Müller, C., Kovacevic, A., et al. (2017). A competitive inhibitory circuit for selection of active and passive fear responses. Nature *542*, 96–100. https://doi.org/10.1038/nature21047.

57. Lee, J.H., Lee, S., and Kim, J.H. (2017). Amygdala Circuits for Fear Memory: A Key Role for Dopamine Regulation. Neuroscientist *23*, 542–553. https://doi.org/10.1177/1073858416679936.
58. Banerjee, S.B., Gutzeit, V.A., Baman, J., Aoued, H.S., Doshi, N.K., Liu, R.C., and Ressler, K.J. (2017). Perineuronal Nets in the Adult Sensory Cortex Are Necessary for Fear Learning. Neuron *95*, 169–179.e3. https://doi.org/10.1016/j.neuron.2017.06.007.
59. Letzkus, J.J., Wolff, S.B.E., Meyer, E.M.M., Tovote, P., Courtin, J., Herry, C., and Lüthi, A. (2011). A disinhibitory microcircuit for associative fear learning in the auditory cortex. Nature *480*, 331–335. https://doi.org/10.1038/nature10674.
60. Li, X.F., Stutzmann, G.E., and LeDoux, J.E. (1996). Convergent but temporally separated inputs to lateral amygdala neurons from the auditory thalamus and auditory cortex use different postsynaptic receptors: *in vivo* intracellular and extracellular recordings in fear conditioning pathways. Learn. Mem. *3*, 229–242. https://doi.org/10.1101/lm.3.2-3.229.
61. Concina, G., Renna, A., Grosso, A., and Sacchetti, B. (2019). The auditory cortex and the emotional valence of sounds. Neurosci. Biobehav. Rev. *98*, 256–264. https://doi.org/10.1016/j.neubiorev.2019.01.018.
62. Jasmin, L., Burkey, A.R., Card, J.P., and Basbaum, A.I. (1997). Transneuronal labeling of a nociceptive pathway, the spino-(trigemino-)parabrachio-amygdaloid, in the rat. J. Neurosci. *17*, 3751–3765.
63. Sato, M., Ito, M., Nagase, M., Sugimura, Y.K., Takahashi, Y., Watabe, A.M., and Kato, F. (2015). The lateral parabrachial nucleus is actively involved in the acquisition of fear memory in mice. Mol. Brain *8*, 22. https://doi.org/10.1186/s13041-015-0108-z.
64. Campos, C.A., Bowen, A.J., Roman, C.W., and Palmiter, R.D. (2018). Encoding of danger by parabrachial CGRP neurons. Nature *555*, 617–622. https://doi.org/10.1038/nature25511.
65. Carter, M.E., Soden, M.E., Zweifel, L.S., and Palmiter, R.D. (2013). Genetic identification of a neural circuit that suppresses appetite. Nature *503*, 111–114. https://doi.org/10.1038/nature12596.
66. Lu, Y.C., Chen, Y.Z., Wei, Y.Y., He, X.T., Li, X., Hu, W., Yanagawa, Y., Wang, W., Wu, S.X., and Dong, Y.L. (2015). Neurochemical properties of the synapses between the parabrachial nucleus-derived CGRP-positive axonal terminals and the GABAergic neurons in the lateral capsular division of central nucleus of amygdala. Mol. Neurobiol. *51*, 105–118. https://doi.org/10.1007/s12035-014-8713-x.
67. Watabe, A.M., Ochiai, T., Nagase, M., Takahashi, Y., Sato, M., and Kato, F. (2013). Synaptic potentiation in the nociceptive amygdala following fear learning in mice. Mol. Brain *6*, 11. https://doi.org/10.1186/1756-6606-6-11.
68. Bowen, A.J., Huang, Y.W., Chen, J.Y., Pauli, J.L., Campos, C.A., and Palmiter, R.D. (2023). Topographic representation of current and future threats in the mouse nociceptive amygdala. Nat. Commun. *14*, 196. https://doi.org/10.1038/s41467-023-35826-4.
69. Wang, Y., Krabbe, S., Eddison, M., Henry, F.E., Fleishman, G., Lemire, A.L., Wang, L., Korff, W., Tillberg, P.W., Lüthi, A., and Sternson, S.M. (2023). Multimodal mapping of cell types and projections in the central nucleus of the amygdala. Elife *12*, e84262. https://doi.org/10.7554/eLife.84262.
70. Nejati, V., Salehinejad, M.A., and Sabayee, A. (2018). Impaired working memory updating affects memory for emotional and non-emotional materials the same way: evidence from post-traumatic stress disorder (PTSD). Cogn. Process. *19*, 53–62. https://doi.org/10.1007/s10339-017-0837-2.
71. Yoshii, T. (2021). The Role of the Thalamus in Post-Traumatic Stress Disorder. Int. J. Mol. Sci. *22*, 1730. https://doi.org/10.3390/ijms22041730.
72. Yang, B., Jia, Y., Zheng, W., Wang, L., Qi, Q., Qin, W., Li, X., Chen, X., Lu, J., Li, H., et al. (2023). Structural changes in the thalamus and its subregions in regulating different symptoms of posttraumatic stress disorder. Psychiatry Res. Neuroimaging. *335*, 111706. https://doi.org/10.1016/j.pscychresns.2023.111706.
73. Vertes, R.P., Linley, S.B., and Hoover, W.B. (2015). Limbic circuitry of the midline thalamus. Neurosci. Biobehav. Rev. *54*, 89–107. https://doi.org/10.1016/j.neubiorev.2015.01.014.
74. Kirouac, G.J. (2015). Placing the paraventricular nucleus of the thalamus within the brain circuits that control behavior. Neurosci. Biobehav. Rev. *56*, 315–329. https://doi.org/10.1016/j.neubiorev.2015.08.005.
75. Zhu, Y., Nachtrab, G., Keyes, P.C., Allen, W.E., Luo, L., and Chen, X. (2018). Dynamic salience processing in paraventricular thalamus gates associative learning. Science *362*, 423–429. https://doi.org/10.1126/science.aat0481.
76. Li, S., and Kirouac, G.J. (2008). Projections from the paraventricular nucleus of the thalamus to the forebrain, with special emphasis on the extended amygdala. J. Comp. Neurol. *506*, 263–287. https://doi.org/10.1002/cne.21502.
77. Vertes, R.P., and Hoover, W.B. (2008). Projections of the paraventricular and paratenial nuclei of the dorsal midline thalamus in the rat. J. Comp. Neurol. *508*, 212–237. https://doi.org/10.1002/cne.21679.
78. Wilker, S., Pfeiffer, A., Elbert, T., Ovuga, E., Karabatsiakis, A., Krumbholz, A., Thieme, D., Schelling, G., and Kolassa, I.T. (2016). Endocannabinoid concentrations in hair are associated with PTSD symptom severity. Psychoneuroendocrinology *67*, 198–206. https://doi.org/10.1016/j.psyneuen.2016.02.010.
79. Neumeister, A., Normandin, M.D., Pietrzak, R.H., Piomelli, D., Zheng, M.Q., Gujarro-Anton, A., Potenza, M.N., Bailey, C.R., Lin, S.F., Najafzadeh, S., et al. (2013). Elevated brain cannabinoid CB1 receptor availability in post-traumatic stress disorder: a positron emission tomography study. Mol. Psychiatr. *18*, 1034–1040. https://doi.org/10.1038/mp.2013.61.
80. Marsicano, G., Wotjak, C.T., Azad, S.C., Bisogno, T., Rammes, G., Cascio, M.G., Hermann, H., Tang, J., Hofmann, C., Zieglgänsberger, W., et al. (2002). The endogenous cannabinoid system controls extinction of aversive memories. Nature *418*, 530–534. https://doi.org/10.1038/nature00839.
81. Shoshan, N., and Akirav, I. (2017). The effects of cannabinoid receptors activation and glucocorticoid receptors deactivation in the amygdala and hippocampus on the consolidation of a traumatic event. Neurobiol. Learn. Mem. *144*, 248–258. https://doi.org/10.1016/j.nlm.2017.08.004.
82. Shoshan, N., Segev, A., Abush, H., Mizrachi Zer-Aviv, T., and Akirav, I. (2017). Cannabinoids prevent the differential long-term effects of exposure to severe stress on hippocampal- and amygdala-dependent memory and plasticity. Hippocampus *27*, 1093–1109. https://doi.org/10.1002/hipo.22755.
83. Segev, A., Korem, N., Mizrachi Zer-Aviv, T., Abush, H., Lange, R., Sauber, G., Hillard, C.J., and Akirav, I. (2018). Role of endocannabinoids in the hippocampus and amygdala in emotional memory and plasticity. Neuropsychopharmacology *43*, 2017–2027. https://doi.org/10.1038/s41386-018-0135-4.
84. Gray, J.M., Vecchiarelli, H.A., Morena, M., Lee, T.T.Y., Hermanson, D.J., Kim, A.B., McLaughlin, R.J., Hassan, K.I., Kühne, C., Wotjak, C.T., et al. (2015). Corticotropin-releasing hormone drives anandamide hydrolysis in the amygdala to promote anxiety. J. Neurosci. *35*, 3879–3892. https://doi.org/10.1523/JNEUROSCI.2737-14.2015.
85. Natividad, L.A., Buczynski, M.W., Herman, M.A., Kirson, D., Oleata, C.S., Irimia, C., Polis, I., Ciccocioppo, R., Roberto, M., and Parsons, L.H. (2017). Constitutive Increases in Amygdalar Corticotropin-Releasing Factor and Fatty Acid Amide Hydrolase Drive an Anxious Phenotype. Biol. Psychiatr. *82*, 500–510. https://doi.org/10.1016/j.biopsych.2017.01.005.
86. Hillard, C.J., Beatka, M., and Sarvaideo, J. (2016). Endocannabinoid Signaling and the Hypothalamic-Pituitary-Adrenal Axis. Compr. Physiol. *7*, 1–15. https://doi.org/10.1002/cphy.c160005.
87. Gunduz-Cinar, O., Macpherson, K.P., Cinar, R., Gamble-George, J., Sugden, K., Williams, B., Godlewski, G., Ramikie, T.S., Gorka, A.X., Alapafuja, S.O., et al. (2013). Convergent translational evidence of a role for anandamide in amygdala-mediated fear extinction, threat processing and stress-reactivity. Mol. Psychiatr. *18*, 813–823. https://doi.org/10.1038/mp.2012.72.
88. Hill, M.N., Campolongo, P., Yehuda, R., and Patel, S. (2018). Integrating Endocannabinoid Signaling and Cannabinoids into the Biology and Treatment of Posttraumatic Stress Disorder. Neuropsychopharmacology *43*, 80–102. https://doi.org/10.1038/npp.2017.162.
89. Elms, L., Shannon, S., Hughes, S., and Lewis, N. (2019). Cannabidiol in the Treatment of Post-Traumatic Stress Disorder: A Case Series. J. Altern. Complement. Med. *25*, 392–397. https://doi.org/10.1089/acm.2018.0437.
90. Roitman, P., Mechoulam, R., Cooper-Kazaz, R., and Shalev, A. (2014). Preliminary, open-label, pilot study of add-on oral Delta9-tetrahydrocannabinol in chronic post-traumatic stress disorder. Clin. Drug Investig. *34*, 587–591. https://doi.org/10.1007/s40261-014-0212-3.
91. Cameron, C., Watson, D., and Robinson, J. (2014). Use of a synthetic cannabinoid in a correctional population for posttraumatic stress disorder-related insomnia and nightmares, chronic pain, harm reduction, and other indications: a retrospective evaluation. J. Clin. Psychopharmacol. *34*,

559–564. https://doi.org/10.1097/JCP.0000000000000180.
92. Fraser, G.A. (2009). The use of a synthetic cannabinoid in the management of treatment-resistant nightmares in posttraumatic stress disorder (PTSD). CNS Neurosci. Ther. *15*, 84–88. https://doi.org/10.1111/j.1755-5949.2008.00071.x.
93. Jetly, R., Heber, A., Fraser, G., and Boisvert, D. (2015). The efficacy of nabilone, a synthetic cannabinoid, in the treatment of PTSD-associated nightmares: A preliminary randomized, double-blind, placebo-controlled cross-over design study. Psychoneuroendocrinology *51*, 585–588. https://doi.org/10.1016/j.psyneuen.2014.11.002.
94. Calabrese, E.J., and Rubio-Casillas, A. (2018). Biphasic effects of THC in memory and cognition. Eur. J. Clin. Invest. *48*, e12920. https://doi.org/10.1111/eci.12920.
95. Johnson, M.J., Pierce, J.D., Mavandadi, S., Klaus, J., Defelice, D., Ingram, E., and Oslin, D.W. (2016). Mental health symptom severity in cannabis using and non-using Veterans with probable PTSD. J. Affect. Disord. *190*, 439–442. https://doi.org/10.1016/j.jad.2015.10.048.
96. Wilkinson, S.T., Stefanovics, E., and Rosenheck, R.A. (2015). Marijuana use is associated with worse outcomes in symptom severity and violent behavior in patients with posttraumatic stress disorder. J. Clin. Psychiatr. *76*, 1174–1180. https://doi.org/10.4088/JCP.14m09475.
97. Bowers, M.E., and Ressler, K.J. (2015). Interaction between the cholecystokinin and endogenous cannabinoid systems in cued fear expression and extinction retention. Neuropsychopharmacology *40*, 688–700. https://doi.org/10.1038/npp.2014.225.
98. Zingg, B., Chou, X.L., Zhang, Z.G., Mesik, L., Liang, F., Tao, H.W., and Zhang, L.I. (2017). AAV-Mediated Anterograde Transsynaptic Tagging: Mapping Corticocollicular Input-Defined Neural Pathways for Defense Behaviors. Neuron *93*, 33–47. https://doi.org/10.1016/j.neuron.2016.11.045.
99. Melo-Thomas, L., Gil-Martínez, A.L., Cuenca, L., Estrada, C., Gonzalez-Cuello, A., Schwarting, R.K., and Herrero, M.T. (2018). Electrical stimulation or MK-801 in the inferior colliculus improve motor deficits in MPTP-treated mice. Neurotoxicology *65*, 38–43. https://doi.org/10.1016/j.neuro.2018.01.004.
100. Fukumoto, K., Iijima, M., and Chaki, S. (2016). The Antidepressant Effects of an mGlu2/3 Receptor Antagonist and Ketamine Require AMPA Receptor Stimulation in the mPFC and Subsequent Activation of the 5-HT Neurons in the DRN. Neuropsychopharmacology *41*, 1046–1056. https://doi.org/10.1038/npp.2015.233.
101. Deolindo, M.V., Reis, D.G., Crestani, C.C., Tavares, R.F., Resstel, L.B.M., and Corrêa, F.M.A. (2013). NMDA receptors in the lateral hypothalamus have an inhibitory influence on the tachycardiac response to acute restraint stress in rats. Eur. J. Neurosci. *38*, 2374–2381. https://doi.org/10.1111/ejn.12246.
102. Ratano, P., Everitt, B.J., and Milton, A.L. (2014). The CB1 receptor antagonist AM251 impairs reconsolidation of pavlovian fear memory in the rat basolateral amygdala. Neuropsychopharmacology *39*, 2529–2537. https://doi.org/10.1038/npp.2014.103.
103. Kuhnert, S., Meyer, C., and Koch, M. (2013). Involvement of cannabinoid receptors in the amygdala and prefrontal cortex of rats in fear learning, consolidation, retrieval and extinction. Behav. Brain Res. *250*, 274–284. https://doi.org/10.1016/j.bbr.2013.05.002.
104. Chaplan, S.R., Bach, F.W., Pogrel, J.W., Chung, J.M., and Yaksh, T.L. (1994). Quantitative assessment of tactile allodynia in the rat paw. J. Neurosci. Methods *53*, 55–63. https://doi.org/10.1016/0165-0270(94)90144-9.

STAR★METHODS

KEY RESOURCES TABLE

REAGENT or RESOURCE	SOURCE	IDENTIFIER
Antibodies		
Rabbit anti-c-Fos mAb	Cell Signaling technology	Cat#2250S; RRID: AB_2247211
Mouse anti-c-Fos mAb	Abcam	Cat#ab208942; RRID:AB_2747772
Mouse anti-CaMKIIα	Thermo Fisher Scientific	Cat# MA1-048, RRID:AB_325403
Rabbit anti-CB1R	Proteintech	Cat# 17978-1-AP, RRID:AB_10859098
Rabbit anti-GAPDH	Proteintech	Cat# 10494-1-AP, RRID:AB_2263076
Rabbit anti-β-actin	Proteintech	Cat# AF7018, RRID:AB_2839420)
Alexa Fluor 488 donkey anti-Mouse IgG (H + L)	Thermo Fisher Scientific	Cat# A-21202, RRID:AB_141607)
Alexa Fluor 594 donkey anti-Rabbit IgG (H + L)	Thermo Fisher Scientific	Cat# A-21207, RRID:AB_141637
Alexa Fluor 488 donkey anti-Rabbit IgG (H + L)	Thermo Fisher Scientific	Cat# A32790, RRID:AB_2762833)
Bacterial and virus strains		
rAAV-EF1α-flex-taCasp3-TEVp-WPRE-hGH polyA, AAV2/9	BrainVTA	Cat#PT-0206
rAAV-Ef1α-DIO-mCherry-WPRE-hGH polyA, AAV2/9	BrainVTA	Cat#PT-0013
rAAV-EF1α-DIO-FLP-WPRE-hGH polyA, AAV2/1	BrainVTA	Cat#PT-0075
rAAV-nEf1α-FDIO-mCherry-WPRE-hGH polyA, AAV2/9	BrainVTA	Cat#PT-0339
rAAV-fSST-CRE-bGH polyA, AAV2/9	BrainVTA	Cat#PT-0279
rAAV-SST-mCherry-WPRE-bGH polyA, AAV2/9	BrainVTA	Cat#PT-1215
rAAV-EF1α-DIO-eNpHR3.0-mCherry-WPRE-hGH polyA, AAV2/9	BrainVTA	Cat#PT-0007
rAAV-CaMKIIa-eNpHR3.0-mCherry-WPRE-hGH polyA, AAV2/9	BrainVTA	Cat#PT-0009
rAAV-CaMKIIa-hChR2(H134R)-EYFP-WPRE-hGH polyA, AAV2/9	BrainVTA	Cat#PT-0296
rAAV-nEF1a-fDIO-eNpHR3.0-mCherry-WPRE-hGH polyA, AAV2/9	BrainVTA	Cat#PT-1261
rAAV-CaMKIIa-mCherry-WPRE-hGH polyA, AAV2/9	BrainVTA	Cat#PT-0108
rAAV-CaMKIIa-CRE-WPRE-hGH polyA, AAV2/9,Retro	BrainVTA	Cat#PT-0220
rAAV-EF1α-DIO-hM4D(Gi)-mCherry-WPREs	BrainVTA	Cat#PT-0043
rAAV-CaMKIIa-EGFP-WPRE-hGH polyA	BrainVTA	Cat#PT-0290
Chemicals, peptides, and recombinant proteins		
MK-801	Tocris	Cat#77086-22-7
NBQX	Tocris	Cat#118876-58-7
WIN55,212-2	Tocris	Cat#131543-23-2
AM251	Tocris	Cat#183232-66-8
Lidocaine	Harvest	N/A
Red Retrobeads	Lumafluor	Cat#78R170
Critical commercial assays		
Synaptic Protein Extraction Reagent	Thermo Fisher Scientific	Cat#87793

(*Continued on next page*)

Continued

REAGENT or RESOURCE	SOURCE	IDENTIFIER
Spin Column Animal Total RNA Purification Kit	Sangon Biotech	Cat#B518561
PrimeScript RT reagent Kit	TakaRa	Cat#RR037A
TB Green Premix Ex Taq II	TaKaRa	Cat#RR820A
Experimental models: Cell lines		
Mouse: C57	Experimental Animal Center of Jinan Pengyue	N/A
Mouse: Vgat-Cre: STOCK Slc32a1$^{tm2(cre)Lowl}$/J	The Jackson Laboratory	JAX: 016962
Oligonucleotides		
PCR Primer : CaMKIIα Forward : GTGTTGCTAACCCTCTACTTTCTC Reverse : ACTTTGGTGTCTTCGTCCTCA	Sangon Biotech	N/A
PCR Primer : FAAH Forward : CCCTGCTCCAACTGGTACAG Reverse : TCACAGTCAGTCAGATAGGAGG	Sangon Biotech	N/A
PCR Primer : CB1R Forward : AAGTCGATCTTAGACGGCCTT Reverse : TCCTAATTTGGATGCCATGTCTC	Sangon Biotech	N/A
PCR Primer : Actin Forward : CTCTCCCTCACGCCATC Reverse : ACGCACGATTTCCCTCTC	Sangon Biotech	N/A
SiRNA sequence : CB1R Sense : GACAUUCAGUACGAAGAUATT Antisense : UAUCUUCGUACUGAAUGUCTT	Genepharma	N/A
Negative Control Sense : UUCUCCGAACGUGUCACGUTT Antisense: ACGUGACACGUUCGGAGAATT	Genepharma	N/A
Software and algorithms		
FV10-ASW	Olympus	N/A
ImageJ software	NIH	RRID:SCR_003070
GraphPad Prism 7	GraphPad	N/A
SPSS 19.0	IBM	N/A
Other		
Optical fibers	inper	N/A

EXPERIMENTAL MODEL AND STUDY PARTICIPANT DETAILS

Animals

We used young adult (7–8 weeks old) C57BL/6J and Vgat-Cre mice in this study. Male C57BL/6J mice were obtained from a commercial supplier (Jinan, Shandong, China) and the Vgat-Cre mice were obtained from Jackson Laboratory and bred at the Experimental Animal Center of Xuzhou Medical University (Xuzhou, China). Mice were allowed to accommodate to the housing environment for 1 week upon arrival before the experiments. The mice were group housed (12 h light/dark cycle) in individually ventilated cages under controlled conditions of temperature (22°C) and humidity (50%) with *ad libitum* access to food and water. Animal experiments were all conducted during the light phase of the cycle. Mice were handled for 3 minutes per day for 3 days before any procedures. All procedures were conducted in accordance with the NIH Guide for the Care and Use of Laboratory Animals (2011) and with full approval from the Institutional Animal Care and Use Committee at Xuzhou Medical University. The study approval number is 202210S043.

Fear conditioning and testing

The fear conditioning paradigm was conducted as previously described with minor modifications.[22] Mice were subjected to habituation and conditioning on specific days in a training context (Context A). Context A consisted of the context chamber illuminated by an overhead house

light and an infrared light and equipped with a speaker to deliver the tone stimuli. The side and back walls of the Context A chamber were covered with black polyester fiber panels and the stainless steel grid floor was connected to a shock generator and was cleaned with 75% ethanol. Distinct from Context A, the side and back walls of Context B were covered with white polyester fiber panels and the floor was a white Plexiglas board. In addition, the walls and floor of Context B were wiped with 10% acetic acid so that the scent differed from Context A. Fear conditioning was performed with the Med Associates Near-Infrared Video Fear Conditioning System (Georgia, VT). On day 1, mice were first acclimated to the behavioral laboratory for 30 minutes, then they were allowed to individually explore the Context A chamber during a 10 min pre-exposure session. On day 2, after 30 minutes of acclimatization in the behavioral laboratory, mice were randomly divided into the FC and Control groups for training. Mice in the FC group were placed in Context A where they were allowed 60 s exploration to record baseline freezing levels, followed by three tones (90 dB, 8000 Hz, 30 s each) delivered with an interval of 210 s; each of the three tones (CS) co-terminated with a 1-s, 1-mA foot shock (US). Mice in the Control group were conditioned individually via a similar protocol, except that the tones did not co-terminate with foot shocks. At the end of the training, mice were put back in their home cages. After 24 h, mice were re-introduced to the Context A chamber for a 5-min contextual test, with no tone stimuli or foot shocks presented. At least 2 h later, mice were placed in the Context B chamber (as described above). After a 60-s exploration period to establish baseline behaviors, a 30-s tone CS was presented and freezing levels were recorded. All the behaviors were acquired by a near-infrared FireWire video camera attached to a computer.

Freezing time calculation

The percentage of time freezing was calculated by comparing the freezing time to the duration of each session. Freezing was defined as the complete absence of movement except for respiratory movements and was automatically scored by the video-tracking software and validated with manual scoring. For fear training, the freezing percentage scored before presentation of the CS (i.e., the baseline freezing) was denoted as CS0 and the freezing levels during first, second, and third CS presentations were respectively denoted as CS1, CS2, and CS3. For the contextual fear memory test, the freezing percentage was determined by the freezing time across the duration of the test session. For the cued fear memory test, the freezing percentage was scored before (pre-Tone) and during tone presentations.

METHOD DETAILS

Stereotactic surgery

Stereotactic brain injections were performed with mice secured in a stereotaxic apparatus (RWD) under 1% pentobarbital anesthesia 60mg/kg. A volume of 200–300 nl of viruses was bilaterally injected using a glass microelectrode (WPI) attached to a 10 μl Hamilton microsyringe at a speed of 50 nl/min, under the control of an infusion pump (KD Scientific). The needle remained in the target site for 10 min after the infusion to prevent the excessive diffusion of the viruses. Mice were placed on a heating pad to maintain a constant temperature throughout the procedure. The coordinates of each injection were measured according to the following elements: AP from bregma, ML from the midline, and DV from the skull surface. The accuracy of virus localization was histologically verified and the behavioral data obtained from mice with injections outside the target region was discarded.

For the pro-apoptosis experiments, rAAV-EF1α-flex-taCasp3-TEVp-WPRE-hGH polyA (AAV-flex-taCasp3, 2.26×10^{12} vg/ml) mixed with rAAV-Ef1α-DIO-mCherry-WPRE-hGH polyA (AAV-DIO-mCherry, 2.88×10^{12} vg/ml) was injected into the CeL (AP: −1.35 mm; ML: ±2.85 mm; DV: −4.75 mm) of Vgat-Cre mice to induce apoptosis in CeL GABAergic neurons. Mice were allowed 3 weeks for viral expression and were then exposed to fear conditioning for behavioral tests. AAV-DIO-mCherry virus was used as the control.

For retrograde tracing, red retrobeads (Lumafluor) were injected into the CeL of C57 mice for retrograde labeling of upstream nuclei. After 2 weeks, mice were transcardially perfused and the fluorescently labeled brain sections were prepared for co-staining with anti-CaMKIIα (1:200) to verify the anatomical connections in the LPB^{Glu}→CeL and PVT^{Glu}→CeL pathways. For transsynaptic anterograde tracing, rAAV-EF1α-DIO-FLP-WPRE-hGH polyA (AAV-DIO-FLP, 1.12×10^{13} vg/ml), a virus that can spread to postsynaptic neurons, was injected into the LPB (AP: −5.15 mm; ML: ±1.35 mm; DV: −3.60 mm) or the PVT (AP: −1.2 mm; ML: ±0.15 mm; DV: −3.4 mm; angled at 4°) of C57 mice. Simultaneously, a mixture of rAAV-nEf1α-FDIO-mCherry-WPRE-hGH polyA (AAV-fDIO-mCherry, 2.25×10^{12} vg/ml) and rAAV-fSST-CRE-bGH polyA (AAV-fSST-CRE, 2.52×10^{13} vg/ml) was delivered to the CeL. The specificity of AAV-fSST-cre in labelling SST positive neurons has been verified in a recent published report, which demonstrated that 74.47% neurons expressing AAV-SST-Cre were SOM^+ GABAergic neurons via immunohistochemistry.[32] Neurons that expressed mCherry were denoted as SOM^+ neurons that were directly innervated by the LPB (or PVT). Four to five weeks later, mice were sacrificed and brain sections were prepared to verify that glutamatergic neurons in the LPB and PVT projected directly to SOM^+ neurons in the CeL. For further confirmation of the LPB→CeL and PVT→CeL projections, rAAV-CaMKIIa-EGFP-WPRE-hGH polyA (AAV-CaMKIIα-EGFP, 6.62×10^{12} vg/ml) was injected into the LPB or PVT, and rAAV-SST-mCherry-WPRE-bGH polyA (AAV-SST-mCherry, 2.58×10^{12} vg/ml) was infused into the CeL to examine the relationship between LPB or PVT glutamatergic nerve terminals and SOM^+ neuronal cell bodies within the CeL.

For optogenetic inhibition of the SOM^+ neurons in the CeL, rAAV-EF1α-DIO-eNpHR3.0-mCherry-WPRE-hGH polyA (AAV-DIO-eNpHR3.0, 2.07×10^{12} vg/ml) and AAV-fSST-CRE were injected into the CeL, followed by bilateral implantation of optical fibers dorsal to the CeL (AP: −1.35 mm; ML: ±2.85 mm; DV: −4.50 mm). Dental cement was used to fix the optical fibers to the skull. For manipulation of the terminals, rAAV-CaMKIIa-eNpHR3.0-mCherry-WPRE-hGH polyA (AAV-CaMKIIα-eNpHR3.0-mcherry, 2.92×10^{12} vg/ml) was injected into the LPB or PVT of C57 mice and optical fibers were inserted into the CeL, which was confirmed to be a downstream area of the LPB and PVT. For manipulation of LPB neurons that project directly to SOM^+ CeL neurons, the FLP-dependent virus rAAV-nEF1a-fDIO-eNpHR3.0-mCherry-WPRE-hGH

polyA (AAV-fDIO-eNpHR3.0-mCherry, 5.16 × 10^{12} vg/ml), mixed with AAV-fSST-Cre was injected into the CeL, and then the Cre-dependent AAV-DIO-FLP was delivered into the LPB for anterograde trans-synaptic transmission, thus driving FLP-dependent transgene expression in SOM^+ CeL neurons.[98] Optical fibers were implanted above the CeL according to the procedures described above. AAV-DIO-mCherry, rAAV-CaMKIIa-mCherry-WPRE-hGH polyA (AAV-CaMKIIα-mcherry, 4.12 × 10^{12} vg/ml) and AAV-fDIO-mCherry viruses were used as the corresponding controls.

For chemogenetic inhibition of CeL-projecting LPB or PVT glutamatergic neurons, rAAV-CaMKIIa-CRE-WPRE-hGH polyA, Retro (Retro-AAV-CaMKIIα-cre, 2.0 × 10^{12} vg/ml) was injected into the CeL, and a Cre-inducible DREADD, rAAV-EF1α-DIO-hM4D(Gi)-mCherry-WPREs (AAV-DIO-hM4Di-mCherry, 3.69 × 10^{13} vg/ml), or the control (AAV-DIO-mCherry) was delivered to the LPB or PVT. Three weeks after the injection, mice received intraperitoneal injection of CNO (3 mg per kg) 45 min before the behavioral experiments. All the viruses mentioned above were purchased from BrainVTA.

For spatially and temporally specific disruption of CB1R expression at LPB→CeL synapses, we developed a small interfering RNA (siRNA) targeting CB1Rs. The brain region for CB1R cleavage was selected by targeting the siRNA injection. We validated the specificity and efficiency of the siRNA via qRT-PCR and western blotting. The NC was set as the control for the siRNA. The siRNA targeting CB1Rs accompanied with the NC were purchased from GenePharma. The viruses mentioned above are listed in the key resources table.

In vivo optogenetic manipulations

To apply optogenetic inhibition during fear conditioning, mice expressing halorhodopsin (eNpHR) in the CeL received three cycles of 90-s optogenetic inhibition (561 nm, 5 mW, constant) with a 150-s interval between cycles. Laser light emitted by a laser generator was transmitted to the target brain area through the patch cords (200-μm core, Newdoon) and optical fibers (200-μm core, Inper), which allowed us to inhibit target neurons with yellow laser light delivered during fear conditioning. Mice expressing only mCherry in the CeL underwent identical laser stimulation to control for nonspecific effects of the laser. Mice were familiarized with the patch cords for at least 3 days before the behavioral experiments.

In vivo pharmacological experiments

Bilateral cannulas targeting the CeL were implanted via stereotactic surgeries as described above, and mice were allowed at least 1 week to recover from the surgery. Thirty minutes before the behavioral tests, an injector was placed inside the cannula and 150 nl of the subsequently indicated drugs was infused into CeL with a pump. Lidocaine (2 μg/side, Harvest) was used to inhibit Na^+ channels and hence to inactivate the CeL. The NMDA receptor antagonist MK-801 (0.2 μg/side) and the non-NMDA receptor antagonist NBQX (0.1 μg/side) were applied to decrease excitatory transmission to the CeL. The dosage of MK-801 was selected according to the recent research data.[99] Likewise, the dosage of NBQX was determined based on previous studies.[100,101] WIN55,212-2 (1 μg/side) was used to activate CB1Rs and AM251 (0.5 μg/side) was used to inhibit CB1Rs. The doses of WIN55,212-2 and AM251 was selected on the basis of previous reports.[102,103] NBQX and AM251 were dissolved in 1%DMSO, whereas WIN55,212-2 was dissolved in 10%DMSO. And MK-801 was dissolved in 0.9% saline. Mice were injected with the solvent for dissolving the above drugs as the control, denoted as the vehicle groups. All drugs were purchased from Tocris Bioscience unless otherwise stated. The chemicals mentioned above are listed in the key resources table.

Immunohistochemistry

Mice were deeply anesthetized with intraperitoneal injections of pentobarbital at 60 mg per kg and then transcardially perfused with 0.9% saline followed by 4% paraformaldehyde (PFA). Brains were removed, post-fixed in 4% PFA overnight at 4°C and then cryoprotected in 30% sucrose solution until they sank. Coronal brain sections were prepared with a cryostat (CM1860, Leica) at a thickness of 30 μm.

For c-Fos immunohistochemistry, brain sections were pretreated with 1% hydrogen peroxide solution for 10 min, blocked with 10% normal donkey serum (VF9003, VICMED) for 2 h at room temperature, and then incubated in a rabbit c-Fos antibody (1:1000) for 24 h at 4°C. After three washes in PBS, the sections were incubated with the biotinylated secondary antibody (PV-9001, zsbio) according to the manufacturer's standard protocols. After three rinses, brain sections were developed in 10% diaminobenzidine (DAB) with 0.01% hydrogen peroxide.

For immunofluorescence, the sections were rinsed three times in PBS, and blocked in 10% normal donkey serum for 2 h before incubation with primary antibodies diluted in blocking buffer, including mouse anti-CaMKIIα (1:200), rabbit anti-c-Fos (1:500), mouse anti-c-Fos (1:500), and rabbit anti-CB1R (1:100) for 48 h at 4°C. Subsequently, brain sections were washed three times for 10 min, and incubated with the corresponding secondary antibodies, such as Alexa Fluor 488 anti-rabbit (1:200), Alexa Fluor 594 anti-rabbit (1:200) and Alexa Fluor 488 anti-mouse (1:200), for 2 h at room temperature. Following three washes in PBS, brain sections were mounted on slides and counterstained with DAPI staining solution to label the nuclei before covering with coverslips The antibodies mentioned above are listed in the key resources table.

Western blotting

Mice were decapitated under isoflurane anesthesia, and their brains were quickly removed to an ice-cooled cryostat for isolation of brain regions. For total protein extraction, dissected tissues were homogenized using an electric homogenizer in RIPA lysis buffer (P00138, Biyuntian) with the phosphatase inhibitor PMSF (ST506, Biyuntian), followed by centrifugation of the tissue homogenates (Eppendorf) at 12,000 rpm for 15 min at 4°C. For synapse-associated protein extraction, separated brain tissues were rapidly immersed and homogenized in the lysate

Syn-PERTM Synaptic Protein Extraction Reagent with PMSF, then centrifuged at 8000 rpm for 10 min at 4°C. Then the sampled supernatants were recentrifuged at 12,000 rpm for 20 minutes, with the cracking buffer added to the particles to acquire the cytoplasmic fraction. Protein concentrations were detected with the bicinchoninic acid assay (P0010, Biyuntian) and adjusted to the identical concentration. Equal quantities of protein samples were separated by 10 % SDS-PAGE gels (PG112, Epizyme) and then transferred to PVDF membranes (Millipore). After blocking with 5% nonfat milk for 2 h at room temperature, the PVDF membranes were incubated with primary antibodies, including mouse anti-CaMKIIα (1:1000), anti-CB1R (1:1000), anti-GAPDH (1:1000), and anti-β-actin (1:1000), at 4°C overnight. Following three washes in washing buffer, the membranes were incubated with HRP-conjugated secondary antibody (1:1000, Affinity) for 1 h at room temperature and visualized with a BeyoECL Moon kit. Western blotting analyses were performed with ImageJ software (NIH). The gray values of targeted bands were normalized to GAPDH or β-actin, and the control group was set as 1. The antibodies mentioned above are listed in the key resources table.

Quantitative reverse transcription polymerase chain reaction (qRT-PCR)

Frozen tissue samples were dissected from the mouse brains, and the total RNA fraction was extracted with a Spin Column Animal Total RNA Purification Kit (Shenggong, China) following the manufacturer's instructions. The concentration and purity of RNA were determined using a NanoDrop-1000 spectrophotometer (ThermoFisher Scientific), followed by the RNA preparations reverse-transcribed to cDNA in parallel with the PrimeScript RT reagent kit as per standard protocols. The cDNA products were served as templates for real-time PCR analysis using the TB Green *Premix Ex Taq* II. Reaction protocols were as follows: 1 min at 95°C for enzyme activation, 40 cycles of 10 s at 95°C, 30 s at 60°C and 30 s at 72°C for PCR reactions, followed by 5 s at 95°C, 60 s at 60°C and 30 s at 50°C for the Melt curve stage. Each assay was performed twice on an Applied Biosystems QuantStudio Real-time PCR system, and expression fold changes were determined using the ΔCt method ($2^{-\Delta\Delta Ct}$), with actin as an endogenous control.

In vitro electrophysiological recordings

For brain slice recordings, mice were perfused transcardially with 15 ml ice-cold high-sucrose cutting solution that contained (in mM) 80 NaCl, 3.5 KCl, 4.5 $MgSO_4$, 0.5 $CaCl_2$, 1.25 NaH_2PO_4, 90 sucrose, 25 NaHCO3, 10 glucose (pH: 7.35, osmolarity: 295–305 mOsm) under deep anesthesia with sodium pentobarbital (60 mg/kg body weight). Coronal slices (300 μm) containing the CeL were sectioned in cutting buffer using a vibratome (VT1200S, Leica, Germany), followed by incubation in high-sucrose cutting solution at 32°C for 1 h. The brain slices were subsequently transferred to a storage chamber containing artificial cerebrospinal fluid (ACSF) for recovery to room temperature before perfusion with ACSF for slice recording. The ACSF (in mM) comprised of 126 NaCl, 2.5 KCl, 1.2 NaH_2PO_4, 1.2 $MgSO_4$, 26 $NaHCO_3$, 10 glucose and 2.4 $CaCl_2$ (pH: 7.35, osmolarity: 295–305 mOsm). All solutions were saturated with 95% O_2 and 5% CO_2.

Patch-clamp recordings were performed in visually identified SOM^+ neurons in the CeL. Thick-walled borosilicate glass pipettes (BF-150-86-10, Sutter, USA) were filled with potassium gluconate-based internal solution containing (in mM): 135 K gluconate, 10 HEPES, 5 EGTA, 3 ATP-Mg, 0.2 GTP-Na, 0.5 $CaCl_2$ and 2 $MgCl_2$ (pH: 7.25, osmolarity: 280–290 mOsm). Patch pipette resistance values were 6–8 MΩ. The signals were obtained from a MultiClamp 700B amplifier (Axon Instruments, Union City, CA, USA), digitized at 10 HZ, and analyzed with Clampex and Clampfit 10 (Axon Instruments, San Jose, CA, USA). For recording of current-evoked firing rates, stepped current input stimuli (0–300 pA;δ = 10 pA) were applied in current-clamp mode. For the plasticity experiments, mEPSCs were recorded in the presence of tetrodotoxin (1 μM) and picrotoxin (100 μM) under voltage-clamp mode at a holding potential of −60 mV. To evoke LPB-driven synaptic transmission onto CeL^{SOM} neurons via ChR2 virus, photostimulation (473 nm, 20 Hz) was delivered and postsynaptic recordings were conducted in the CeL areas with ChR2 terminal expression. For drug treatments, only photo-responsive CeL neurons were recorded and investigated for postsynaptic responses to the CB1R agonist and antagonist. The concentrations of the drugs applied in the electrophysiological recordings were WIN55,212-2 (5 μM) and AM251 (2 μM).

RNAscope *in situ* hybridization

An RNAscope multiplex fluorescent reagent kit and appropriately designed probes (Genepharma, China) were used in this study. Mice were perfused as depicted in immunohistochemistry, and mouse brains were post-fixed in 4% PFA for 12 h. After cryoprotection with 30% sucrose for 2 days, the brain sections were prepared at a thickness of 20 μm with a cryostat and attached onto microscope slides. For reactivation of the cells, the brain sections were incubated with citrate buffer for 15 min at RT. Sections were washed 2× in DEPC-PBS for 5 min. Sections were then incubated at 37°C for 30 min with Proteinase K to enhance tissue permeability and nucleic acid probe penetration. Without washes, sections were incubated at 37°C with blocking buffer for 30 min. Following three washes in 2× SSC for 1 min at RT, brain sections were incubated at 78°C for 8 min in denaturation solution (containing deionized formamide, 2× SSC, and H_2O-DEPC). Then the brain sections were dehydrated through an ethanol series (70%, 80%, 90%, 100% in each Coplin jar) for 2 min in each jar. The probes labeled with biotin were denatured for 10 min at 75°C, and SA Cy3 dye labeled with red fluorescence or SA FAM dye labeled with green fluorescence accompanied with PBS were added in a determined proportion to prepare the probe working solution. The working solution mixed with the pre-warmed hybridization buffer, and the sections were then hybridized in this solution at 37°C for 16 h in a humidified chamber. After hybridization, brain sections were washed in wash buffer for 15 min, followed by three washes at 60°C for 10 min, and three washes at 37°C for 10 min in 2× SSC. Finally, a DAPI counterstain was applied onto the slides over the hybridization area, and incubated for 20 min at RT in a light-proof box. After two washes in DEPC-PBS for 2 min, the specimen was ready for visualization by fluorescent microscopy.

Von Frey filament test

Mechanical pain thresholds were measured with von Frey filaments according to Dixon's up–down method as described in a previous report.[104] Before the behavioral test, each mouse was placed in a Plexiglas box on a wire mesh grid for 1 h to acclimate to the testing environment. Calibrated von Frey filament hairs were pressed onto the plantar surface of the left hind paws with sufficient force to bend the filaments. A brisk withdrawing or flinching of the hind paw was considered as a positive pain response. In case of paw withdrawal, a filament of weaker force was selected; in the absence of a positive response, a filament of greater force was applied. The mean withdrawal threshold was ultimately calculated as the average of six applications. Pain thresholds were tested 1 min after optogenetic manipulations.

Y-maze test

The Y-maze test was used to assess spatial working memory in mice. The experiment was conducted in a warm and quiet environment and the mice were acclimated to the testing environment for 30 minutes. During training session, the mice were placed into the Y-maze with one arm of the maze closed off and the closed arm was designated as the novel arm. After a certain time interval of 3 hours, mice were placed back into the maze and allowed to explore the maze for 10 minutes with the blockage removed during testing session. The time of entries into the novel arm was calculated and analyzed via Anymaze software.

QUANTIFICATION AND STATISTICAL ANALYSIS

All experiments and statistical analyses were conducted with the investigators blinded, including the behavioral analyses, western blotting, immunohistochemistry, and electrophysiology. Data analyses were performed with SPSS 19.0 (IBM, USA), with graphing conducted in GraphPad Prism 7 (Graph Pad Software). Unpaired two-sample Student's *t*-tests were used to perform two-group comparisons. For multiple comparisons, data were analyzed with one-way and two-way analyses of variance (ANOVA), followed by Bonferroni tests or Tukey post hoc tests for pairwise comparisons in case of significance. Significance levels are displayed as $^{*}P<0.05$, $^{**}P<0.01$, and not significant (NS), and results are expressed as the mean $\pm$ SEM.